Fundamental Research 4 (2024) 1542–1556

Contents lists available at ScienceDirect

Fundamental Research

journal homepage: http://www.keaipublishing.com/en/journals/fundamental-research/

Article

Formation of reactive species via high power microwave induced DNA damage and promoted intrinsic pathway-mediated apoptosis in lung cancer cells: An *in vitro* investigation

Juie Nahushkumar Rana [a,b,1], Sohail Mumtaz [b,c,1], Ihn Han [a,b], Eun Ha Choi [a,b,c,*]

[a] Department of Plasma Bio Display, Kwangwoon University, Seoul 139701, South Korea
[b] Plasma Bioscience Research Center (PBRC), Kwangwoon University, Seoul 139701, South Korea
[c] Department of Electrical and Biological Physics, Kwangwoon University, Seoul 139701, South Korea

ARTICLE INFO

Article history:
Received 10 October 2023
Received in revised form 1 February 2024
Accepted 4 February 2024
Available online 8 February 2024

Keywords:
Non-small cell lung cancer
High power microwave
Microwave DNA damage
Reactive species
Mitochondria dysfunction
Skin depth

ABSTRACT

Lung cancer continues to be the second most common cancer diagnosed and the main cause of cancer-related death globally, which requires novel and effective treatment strategies. When considering treatment options, non-small cell lung cancer (NSCLC) remained a challenge, seeking new therapeutic strategies. High-power microwave (HPM) progressions have facilitated the advancement of new technologies as well as improvements to those already in use. The impact of HPM on NSCLC has not been investigated before. In this work, we uncovered the effect of pulsed HPM on NSCLC (H460 and A549) for the first time and the most likely underlying mechanisms. Two NSCLC (H460 and A549) cells and lung normal MRC5 were exposed to HPM (15, 30, 45, and 60) pulses (2.1 mJ/pulse). After exposure, the effects were observed at 12, 24, 48, and 72 h. HPM primarily increases the level of intracellular reactive species by a strong electric field of ~27 kV/cm, which altered NSCLC viability, mitochondrial activity, and death rates. A model for the production of intracellular reactive species by HPM was also presented. NSCLC is found to be affected by HPM through DNA damage (upregulation of ATR/ATM, Chk1/Chk2, and P53) and increased expression of apoptotic markers. NAC scavenger and CPTIO-inhibitor confirm that the reactive species are mainly accountable for cellular effects. In order to ensure suitability for real-world usage, the skin depth was calculated as 30 mm. ROS played a main role in inducing cellular effects, with NO species possibly playing a contributing role. These findings clarify the cellular mechanisms underlying HPM-induced cell death, potentially advancing therapeutic approaches for treating NSCLC, and a useful first step for future investigations in this area. Moreover, this technique has the potential to serve as an adjunct to non-surgical methods in cancer therapy.

1. Introduction

The widespread use of microwaves frequently encourages researchers to look into both their positive and negative effects. These are known as non-ionizing radiation and are placed next to infrared in the electromagnetic (EM) spectrum. Besides its domestic use, many other applications of microwaves in several fields have been identified which strongly depend on the amount of EM energy and their specific frequency [1]. Progress in high-power microwaves (HPM) introduces innovative technologies and improvements in existing ones. The ability of microwaves to detect tumors at an early stage, blood clot/stroke detection, early-stage breast cancer, heart imaging, and bone imaging gives it sustainable value in the medical field [2–9]. Chronic microwave exposure is crucial for biological processes like detecting intracranial hematomas and accelerating wound healing [2–9]. In most cases, microwaves can also be employed to suppress cancers [10–12]. The effects of thermal and non-thermal microwaves have been studied on cellular and protein activity levels [13,14].

Lung cancer is a significant health concern worldwide, as it is the second most frequently diagnosed cancer and the leading cause of cancer-related deaths. Therefore, there is a need for innovative and effective therapeutic interventions to address this issue [15,16]. Although many different methods have been used to treat lung cancer, the survival rate is still below a year. Recently, microwave therapy has also been implemented in clinics for the treatment of different cancers [10–12]. According to reports, microwave causes tumor cells to undergo apoptosis [17]. It is noted that patients who receive microwave therapy before surgery exhibit a more favorable prognosis [18]. Recent research reported examining the impact of W-band millimeter-wave radiation, operating at a non-thermal power density of 0.2 mW/cm^2, on the morphological

* Corresponding author.
E-mail address: ehchoi@kw.ac.kr (E.H. Choi).
[1] These authors contributed equally to this work.

https://doi.org/10.1016/j.fmre.2024.02.001

characteristics of human lung cancer cells (H1299) [19]. Specifically, an increase in exposure dosage resulted in a greater alteration of cell morphology [19]. The morphological alterations and cell shrinking in lung cancer A549 cells are observed by microwave radiations which promote cell apoptosis [20]. Among many applications, the microwave technique is adaptable for detection, mapping, and treatment [21,22]. Interesting findings from our most recent research demonstrate that specific doses of HPM pulses induce apoptosis in brain cancer U87-MG cells [23].

Over the past two decades, outcomes for non-small-cell lung cancer (NSCLC) have significantly improved thanks to molecular targeted therapies and immunotherapies. However, the majority of NSCLCs are still difficult to treat because they develop resistance to available therapies, necessitating novel strategies [24]. With our best literature review, no research has been done to determine how pulse HPM (nanosecond pulses) affects NSCLC. For the first time, we observed how HPM pulses affected NSCLC and the most likely underlying mechanisms.

We aimed to investigate the impact of pulsed HPM on lung normal fibroblast MRC5 cells and NSCLC (H460 and A549) in this study. The HPM is generated from a virtual cathode oscillator (vircator) with a frequency of 3.5 GHz. The cells are directly exposed to the HPM radiation by 15, 30, 45, and 60 pulses (2.1 mJ/pulses), and effects were analyzed at 12, 24, 48, and 72h after exposure. Cell death, ATP levels, and metabolic viability were used to analyze the cellular effects. Additionally, a model was presented to elucidate the mechanisms underlying the production of intracellular reactive oxygen species (ROS) and reactive nitrogen species (RNS) in response to HPM irradiation. The molecular and protein expression analysis was used to look into the potential mechanism.

2. Materials and methods

2.1. Cell culture

The Korean Cell Line Bank (Seoul, Korea) was used to purchase two human NSCLC cell lines (A549 and H460) as well as lung normal fibroblast MRC5 cell lines. 10% fetal bovine serum, 100 μg/mL of streptomycin, and 100 U/mL of penicillin were contained in media DMEM (Cat# LM001-05; Welgene, Korea) and RPMI (Cat# LM011-51; Welgene, Korea) and cells were normally culture at 37 ˚C in a humidified incubator with 5% CO_2. These cell lines have been used to investigate the biological effects of HPM on lung cells.

2.2. Metabolic viability/cell cytotoxicity assay

NSCLC (A549 and H460) and lung normal MRC5 cells were selected to assess cell cytotoxicity assay by using reagent Alamar blue dye (DAL1025; Thermo Fisher Scientific, Waltham, MA, USA). In 96-well plates, 1×10^4 cells/ml usually set density for experiments. With control and treated groups, experiments were carried out in at least three replicas. Using a BioTek plate reader and excitation and emission wavelengths of 540 nm and 600 nm, the fluorescence emission of the Alamar blue dye was measured in order to assess conversion.

2.3. Intracellular ATP measurement

According to the manufacturer's instructions, the Cell Titer-Glo Assay (Promega; cat. no. G7572) was used to measure cellular ATP as a sign of cellular health. 96-well plates with 1×10^4 cells per well were used for this. Cells were supplemented with an equal volume of prewarmed reagent after 24 h of incubation, and they were then incubated for 1 h at 37 ˚C. Luminescence measurements were performed using a microplate reader after incubation.

2.4. Extracellular ATP measurement (DAMP)

Cell Titer-Glo (Promega (cat no. G7572)) kit was used to measure extracellular ATP levels known as damage-associated molecular patterns (DAMPs) inside media after HPM treatment. For this, by keeping the density 1×10^4 cells/100 μl in a well, cells were seeded in a 96-well plate. After 24 h of post-incubation with HPM treatment, the cells' supernatant was transferred to another 96-well plate, where they were mixed with an equivalent volume of prewarmed reagent and incubated at 37 ˚C for 1 h. Following the incubation period, luminescence was evaluated using a microplate reader.

2.5. Flow cytometric analysis for cell death

Cells at a density of 2×10^5 cells/ml culture in a 6-well plate to measure the cell death analysis after HPM treatment. HPM at various pulses, such as 15, 30, 45, and 60 given to cells. After treatment for 24 h, the cells were incubated. The FITC Annexin V Apoptosis Detection Kit: BD 556547 was used to resuspend the pellet in PI and Annexin V staining solution, which was then incubated for 15 min on ice. flow cytometer machine is used to analyze the cell death after irradiation to different HPM.

2.6. Intracellular ROS/RNS detection

H460 and MRC5 cells were seeded in 12-well plates at a density of 5×10^4 cells/ml per round glass coverslip and incubated for 24 h at 37 ˚C with 5% CO_2. Then, cells were treated with HPM using different treatment pulses (15, 30, 45, and 60). 2′,7 Dichlorodihydrofluorescein diacetate (H2DCFDA, Invitrogen, CA, USA) was acquired in accordance with the manufacturer's instructions in order to measure intracellular ROS. To assess intracellular RNS level Diamino fluorescein-FM diacetate (DAF-FMDA, Life Technologies D-23844) was applied on cells. Fluorescence images were captured using laser scanning confocal microscopy (Zeiss, LSM 510, Little Rock, AR, USA) at a 40× magnification. The N-acetyl cysteine (NAC) scavenger and CPTIO inhibitor were also used to evaluate the levels of intracellular and extracellular ROS/RNS. NAC was used at a dose of 5 mM to remove reactive species and confirm their role in cellular effects. In addition, we eliminated NO species by using CPTIO at a concentration of 0.1 mM.

2.7. Apoptosis detection in human lung cancer cells by DAPI and PI staining as well as cell migration assay

At a density of 5×10^4 cells/ml seeded on a round glass coverslip, lung cancer (H460) and normal (MRC5) cells were grown in their respective media overnight in 12-well plates. Following that, the cells were kept in an incubator for 24 h at 37 ˚C and 5% CO_2. After that, cells were treated with an HPM treatment. The cells were fixed with 4% paraformaldehyde following a 24-hour incubation period, and then they were washed 1X with sterile PBS. Afterward, stained with propidium iodide (50 μg/ml) and stained for 30 min at room temperature in the dark. Washed 3 times with 1X PBS and then added DAPI (1 mg/ml) for 20 min at room temperature. In order to prevent overstaining, the cells were once more washed with PBS. Fluorescence images were then taken using a laser scanning confocal microscope (Zeiss, LSM 510, Little Rock, AR, USA) at a 20x magnification.

2.8. Migration assay

H460 cells were plated onto 6-well plates at a density of 2×10^5 cells/ml, and they were incubated for 24 h to grow. To remove detached cells from the plate, the wound space was scratched and cells were rinsed with fresh medium. The NSCLC H460 cells were treated with HPM radiations at indicated pulses (15, 30, 45, and 60: 2.1 mJ/pulse). In order to evaluate cell migration, wound closure in response to HPM treatment was observed and photographed under a microscope (Nikon Eclipse Ti, Japan) at intervals of 0 and 24 h. The area of scratch was expressed as 100% at the 0 h time point.

2.9. Quantitative real-time polymerase chain reaction (qRT-PCR)

After HPM treatment cells are subjected to RNA extraction post 24 h incubation. Complementary deoxyribonucleic acid (cDNA) synthesis steps were carried out after RNA extraction. Intrinsic pathway-activated genes were quantified by quantitative real-time polymerase chain reaction (qRT-PCR). The primers included Ataxia-telangiectasia and Rad3-related (ATR), Ataxia-telangiectasia mutated (ATM), Checkpoint kinase 1 (Chk1), Checkpoint kinase 2 (Chk2), BReast CAncer gene 1 (BRCA1), BReast CAncer gene 2 (BRCA2), P53, Cell division cycle 25 (CDC25c), Bcl-2-associated X protein (Bax), Bcl-2 homologous antagonist/killer (Bak), cysteine-aspartic proteases (Caspase), Casapse 3/8, B-cell lymphoma 2 (Bcl2), Fas, Epidermal growth factor (EGF), TNF-related apoptosis-inducing ligand (TRAIL) and Poly (ADP-ribose) polymerase (PARP) (Bionix, Seoul, Korea). In Table S1, the primer sequences were displayed. As a control gene, glyceraldehyde 3-phosphate dehydrogenase (GAPDH) was utilized. For three separate experiments, each reaction was carried out in triplicate.

2.10. Western blotting analysis

For this experiment, cells were seeded in 6-well plates at a density of 2×10^5cells/ml per well after exposure to HPM treatment for selective periods. Following a 24-hour incubation period, the cells were harvested for protein sample collection. Protein extraction was performed, and subsequent quantification was carried out. Sodium dodecyl sulfate-polyacrylamide gel electrophoresis (SDS-PAGE) is frequently utilized to achieve high-resolution separation of complex protein mixtures. To determine the protein expression levels, Western blotting was employed using specific antibodies deemed suitable for the experiment. Multiple antibodies were utilized to confirm DNA damage via P53 and Bax, while GAPDH was utilized as a control.

2.11. Pulsed high-power microwave system and exposure method

2.11.1. High-power microwave system "Chundoong"

For the purpose of producing pulsed HPM, a vircator-based HPM generator "*Chundoong*" was used in this work [25]. The device was schematically presented in Fig. 1A. The diode chamber was evacuated to a high vacuum level of 1×10^{-5} *Torr* [25]. The vacuum diode region consists of three main parts: a metal cathode covered with velvet and having a radius of 4.5 cm, an anodic mesh foil, and a virtual cathode (VC) (Fig. S1 (a–e)). The waveguide's inner radius of 10 cm was the same as the radius of the anodic mesh. The 25 cm long guiding tube had a 1.5 cm thick acrylic seal at one end to keep the vacuum pressure in place. Our previous work provided a comprehensive description of the mechanisms involved in the generation of HPM by the *Chundoong* [25–28].

2.11.2. Experimental setup and exposure method

The cells are cultured in T75 flasks and seeded in 96 well plates at a density of 1×10^4 cells/ml for HPM treatment. Each experiment used two groups of cells: a control group and a treatment group. The control group consisted of cells that were not given any treatment. The treated groups were subjected to a range of HPM exposure, with 15, 30, 45, and 60 pulses applied to samples placed 15 cm from the output window of the HPM generator, as depicted in Fig. 1A. The HPM pulses were delivered directly to the cells. Following the exposure, the control and treated groups were incubated for 12, 24, 48, and 48 h, after which cell viability, ATP levels, and other biological effects of HPM were evaluated in lung normal (MRC5) and lung cancer A549 and H460 cell lines. In order to assess the temperature changes in the cell media following exposure to HPM, a thermometer was utilized. The temperature of the experimental ambient environment was maintained at a constant 25 °C, and the temperature of the media was recorded in the control group as well as after exposure to 15, 30, 45, and 60 pulses of HPM. The pH and EC of the RPMI were determined using a multifunction benchtop meter from Thermo Scientific Orion. Additionally, the ORP of the RPMI was assessed post-HPM treatment using an ExStik meter (Extech, model: RE300, China).

2.12. Statistical analysis

The data obtained from three independent experiments ($n = 3$) were analyzed and represented as the mean standard error using Microsoft Excel software (Microsoft Office 365) and Graph Pad Prism. To evaluate the statistical significance of the results, the student's *t*-test was employed. The observed differences were considered significant if the p-value was less than 0.05. The statistical significance was denoted using asterisks as follows: $^{*}p < 0.05$, $^{**}p < 0.01$, and $^{***}p < 0.001$.

3. Results

3.1. HPM characteristics and their influence on inducing physiological changes in RPMI after irradiation

The cells were directly irradiated to HPM using 15, 30, 45, and 60 pulses (Fig. 1A). Fig. 1B shows the HPM real signal to obtain the frequency which is observed as 3.5 GHz (Fig. 1C). The EM energy "*E*" of a single pulse that is delivered to the cells was estimated as $E = P \times t/2 \cong 2.1$ mJ/pulse, where, P is the power of HPM (59 kW) approaching the sample and $t \cong 70\ ns$ is the pulse duration (Fig. 1D). Another simulation was run using the High-Frequency Structure Simulator (HFSS) to observe the electric field at the sample position. With the help of the HFSS, we were able to observe the electric field in both the air and the vacuum (waveguide) regions, with the results displayed in Fig. 1E. Further details on HPM characteristics were provided in Supplementary material Figs. S1–S4. Consequently, each trigger pulse delivered 2.1 mJ of EM energy to the sample. The cells corresponding to the chosen pulses of 15, 30, 45, and 60 received delivered EM energies of 31.5, 63, 94.5, and 126 mJ (Fig. 1F). The pH (Fig. 1G) and temperature (Fig. 1H) remained unchanged post-exposure. It has been observed that HPM exposure induced a certain amount of reactive oxygen species and reactive nitrogen species (ROS/RNS) when a strong electric field of 27 kV/cm interacted with the cell media (Fig. 1I, J). When cell culture media were exposed to 15, 30, 45, and 60 pulses of HPM, the NO_x concentration dramatically increased to 1.2, 12, 15.3, and 18 μM at 0 h, respectively. Similar to this, after receiving the chosen doses of 15, 30, 45, and 60 HPM pulses, the H_2O_2 increased to 0.6, 0.92, 2.29, and 3.1 μM at 0 h, respectively. The amount of ROS and RNS remained relatively constant for the first 24 h (0–24 h), then gradually decreased with longer incubation times. The findings are consistent with our prior experiment [23]. The ability of the cell culture media to act as a buffer may be the cause of the ROS and RNS content decreasing with increased incubation time. The physiological changes of the cell culture medium (RPMI) can be explained by ORP and EC. The ORP and EC were observed to rise in a dose-dependent manner following HPM irradiation (Fig. 1K, L). Elevated EC values signify higher ion concentrations, which could cause cellular stress and promote the production of ROS. Higher positive ORP values, on the other hand, indicate an oxidizing environment that also stimulates the production of reactive species in RPMI.

3.2. Potential effects of HPM on the cytotoxicity of human lung cancer and normal cells

HPM radiations were employed on human lung normal (MRC5) and lung cancer (H460 and A549) cells and the cytotoxicity of the radiations was determined using the Alamar blue assay. Fig. S5 and S6 show the acceptable treatment window for lung cancer and normal cells. At first, we focused on the safe treatment range where we selected a range of HPM pulses (15, 30, 45, 60, 75, 90, 105, and 120) on three normal cells (MRC5, HGF, and HaCat) and two lung cancer H460 and A549 cells, as illustrated in Supplementary Fig. S5 and S6. It is interesting to note

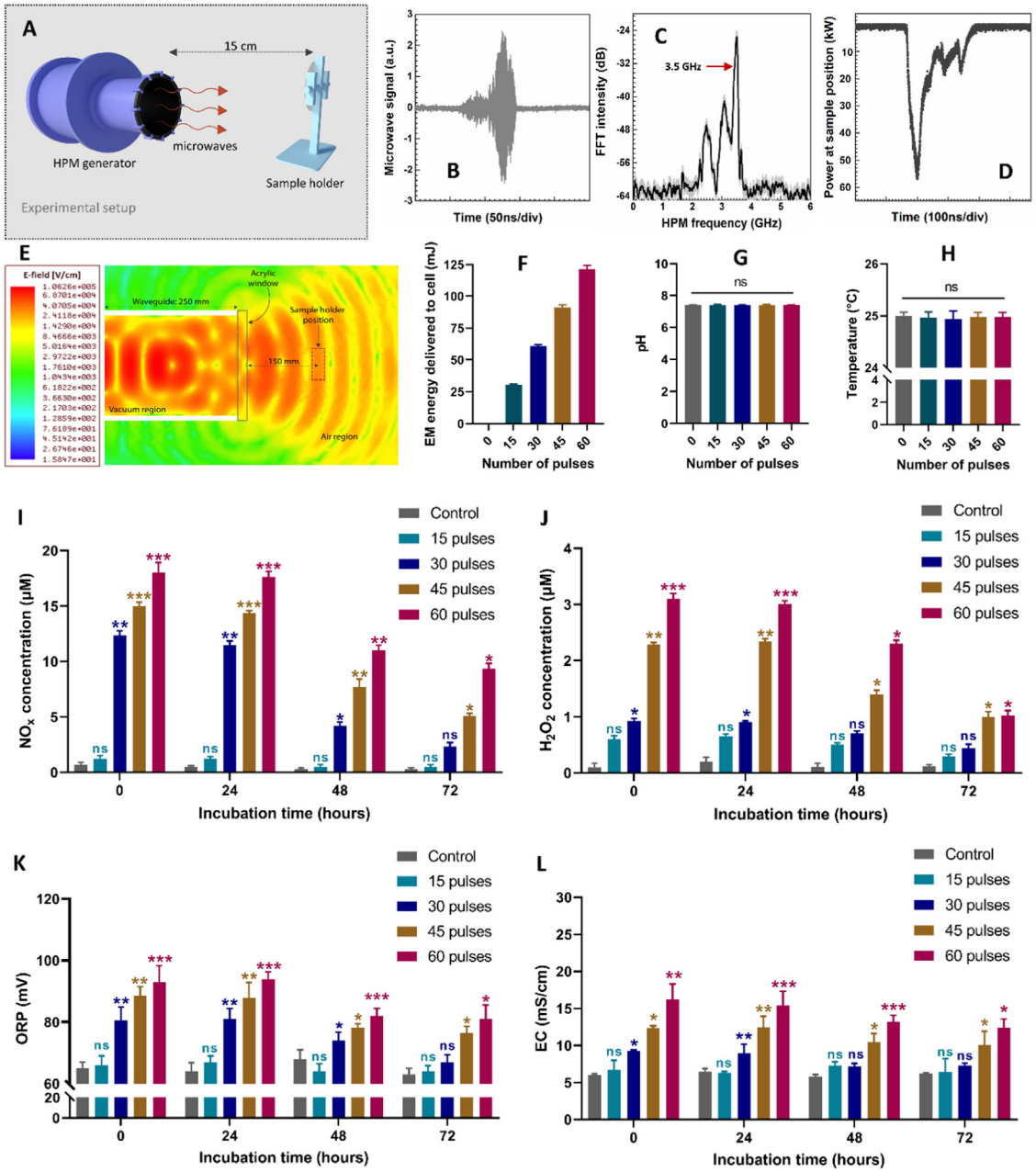

Fig. 1. The experimental setup, properties of pulsed HPM, and physiological changes in the cell culture media after irradiation. (A) Experimental arrangements. (B) HPM signal acquired during the experiment. This HPM real signal was used to analyze the frequency using FFT. (C) The main oscillating frequency was determined to be 3.5 GHz. (D) The HPM envelope signal. The applied HPM had an average power of 59 kW, delivering 2.1 mJ of EM energy to the cells at each pulse. (E) The electric field profile obtained from HFSS simulation, in both the air (sample position) and the vacuum (waveguide) regions. At a single HPM pulse, the electric field is 27 kV/cm at the location of the sample. (F) The cells corresponding to the chosen pulses of 15, 30, 45, and 60 received EM energies of 31.5, 63, 94.5, and 126 mJ. (G) The pH of the cell culture media (RPMI) after HPM irradiations. No change in the pH after HPM exposure at selected doses. (H) The temperature of the media post-exposure. No noticeable changes were observed in the temperature post-exposure. (I) and (J) the concentration of NO_x and H_2O_2 inside the culture media after HPM irradiation. HPM exposure induced a certain amount of NO_x and H_2O_2 when a strong electric field interacted with the cell media. When cell culture media was exposed to 15, 30, 45, and 60 pulses of HPM, the NO_x concentration dramatically increased to 1.2, 12, 15.3, and 18 μM at 0 h, respectively. Similarly, the H_2O_2 concentration increased to 0.6, 0.92, 2.29, and 3.1 μM at 0 h, respectively, post-exposure. The amount of ROS and RNS remained relatively constant for the first 24 h (0–24 h), then gradually decreased with longer incubation times. (K) The ORP of the RPMI post-HPM exposure. Raising the HPM pulses led to a notable rise in the ORP. (L) The EC of media post HPM exposure. Increasing the pulses caused a significant elevation in the EC of the RPMI. Microsoft Excel was used to calculate the significance (MS Office 365). Differences between treatment groups are denoted by $^{*}P < 0.05$, $^{**}P < 0.01$, and $^{***}P < 0.001$.

that up to 75 HPM pulses MRC5 do not show a significant decrease in viabilities where cancer cells decreased 20% to 25%. Exceeding 75 pulses also causes a decrease in the viability of lung normal MRC5 cells (Fig. S5). The results of Fig. S5 indicate that there is an exposure range for each cell at which HPM has no negative effects on healthy cells. However, surpassing the safe dose level may pose a harmful effect on healthy cells.

These findings warrant further investigation into the potential therapeutic applications of HPM. Further study was carried out by using a maximum of 60 pulses. Results were seen at the incubation periods 12,

24, 48, and 72 h after exposure to selected dosages (15, 30, 45, and 60; 2.1 mJ/pulse). Fig. 2 displays the results of the cell viabilities, and intracellular, and extracellular ATP levels after HPM exposure at chosen pulses and incubation times. At all chosen doses and incubation times, it was found that the viability of the normal MRC5 cells remained unaffected. So, it is interesting to note that HPM had no negative effects on MRC5 (Fig. 2A). The viability of lung cancer H460 cells after HPM irradiation was significantly impacted as shown in Fig. 2B. The viability of lung cancer H460 cells was significantly reduced at 24 h after exposure to 45 and 60 HPM pulses, and this effect persisted for 48 and 72 h of incubation. Similarly, the viability of the lung cancer A549 cell line was also evaluated following the HPM exposure and results were provided in Fig. 2C. Up to 45 pulses, HPM had no effect on the viability of the A549 cells at 12 h incubation period, and 60 pulses caused a slight decline. The viability of A549 cells reduced dramatically at 45 and 60 pulses, 24 h after exposure. This effect continued after 48 and 72 h of incubation. H460 exhibits its greatest effect in 45 and 60 pulses after 24 h post-irradiation, but 15 and 30 pulses are not as effective up to 72 h. We noticed that the treatment effects in 45 and 60 pulses after 48 and 72 h incubation exhibit certain distinct phenomena. In contrast, A549 showed a significant decrease at 45 and 60 pulses after a 24 h incubation period. According to these findings, H460 exhibits a considerable decline in viability after being exposed to HPM radiations.

Another crucial parameter to verify the viability of cells is intracellular ATP. After being exposed to HPM with the 15, 30, 45, and 60 pulses, we measured the ATP levels of lung cancer cell lines H460 and A549 as well as lung normal MRC5 cell lines. To support viability results, the intracellular (Fig. 2D–F) and extracellular (Fig. 2G–I) ATP levels were also measured which shows a similar trend to those observed in the viability, and detailed results with explanations were provided in supporting information Fig. S7 and Fig. S8. No signification alterations in intracellular/extracellular ATP levels were evident in lung normal MRC5 cells, even following up to 60 pulses (Fig. 2D, G), when observed 24 h post-exposure. On the other hand, it was found that both lung cancer cell lines (H460 and A549) showed a dose-dependent decrease in intracellular ATP levels 24 h after exposure, as shown in Fig. 2E, F. Damage-associated molecular patterns (DAMPs) are molecules that are released, ejected, or surface-exposed by perishing, stressed, or damaged cells. They are also known as damage cell signals. DAMPs are endogenous signals that are released into the extracellular environment in response to cellular damage brought by treatment. In this work, we have estimated the extracellular ATP in the cell media, which acts as a DAMP signal after HPM exposure. As shown in Fig. 2H, I, extracellular ATP levels also showed dose-dependent increases, indicating cell damage and the release of ATP molecules into the RPMI.

From viability, intracellular ATP, and extracellular ATP results, it can be seen that the HPM pulses significantly change the viability and ATP levels of both lung cancer (H460 and A549) cells, whereas lung normal MRC5 cells were unaffected by the 15, 30, 45, and 60 pulses of HPM radiation. At 24 h after exposure, both cancer cells, in particular the H460 cell line, significantly responded. In this study, we have chosen a 24 h incubation period with the lung-normal MRC5 and lung-cancer H460 cell lines for further research.

3.3. Pulsed HPM irradiation induces cell death via elevated ROS/RNS levels

The effects of pulsed HPM exposure on cell death were evaluated using PI uptake, which is indicative of a damaged plasma membrane. According to the findings (Fig. 3A), HPM pulses do not cause cell death in lung normal MRC5 cells at all selected doses (15, 30, 45, and 60 pulses). Comparing HPM-exposed groups to control groups, however, revealed a number of important differences in the populations of H460 cells. A dose-dependent pattern of cell death in H460 was seen. Maximum cell death was noted following HPM at 60 pulses (Fig. 3A). Fig. 3B and C illustrate the percentage of cell death in MRC5 and H460, including cell survival, early apoptosis, late apoptosis, and necrosis. It is interesting to note that lung cancer H460 cells specifically experienced significant cell death, whereas MRC5 was either unaffected or had negligible effects. Such effects exhibit a significant sign that offers the opportunity to investigate the mechanism underlying dose-dependent cell death in lung cancer H460 cells. Histogram analysis of PI staining in lung cancer cells (H460) is displayed in Fig. 3D. In the lung cancer H460 cell line, ROS levels were seen to rise in a dose-dependent manner. When cells were exposed to HPM radiation pulses with 15, 30, 45, and 60 pulses, a shift in the curve was observed. Our investigation into the intracellular ROS/RNS levels following HPM exposure was aided by this indication.

ROS/RNS-induced oxidative stress can lead to mitochondrial depolarization, ultimately triggering apoptosis. In the case of pulsed HPM exposure, RONS may potentially initiate apoptosis through this mechanism. It was observed that the ROS level in MRC5 only slightly increased after 60 pulses of HPM radiation. After 15, 30, and 45 pulses of HPM radiation in the MRC5, the intracellular RNS/ROS levels remained statistically insignificant and results were provided in supplementary information in Fig. S9. On the other hand, Fig. 3E shows that H460 cells exposed to HPM irradiation had significantly higher levels of ROS/RNS fluorescence levels than the untreated control group. It is also observed that the ROS/RNS intensity in H460 increased in a dose-dependent manner. The ROS/RNS intensity after HPM exposure to 15, 30, 45, and 60 pulses is depicted in Fig. 3F, G. In H460 cells, it was discovered that the ROS/RNS intensity increased in all treated groups when compared to the control (without HPM exposure). The enhancement in intracellular ROS/RNS levels can be explained by HPM as shown schematically in Fig. 3H. When the electric field $E = 27\ \mathrm{kV/cm}$ produced by HPM interacting with cell membrane components (chemical composition), cytoplasm, and mitochondria, the intracellular ROS/RNS can be formed. It is also conceivable that exposure to HPM may have triggered cellular pathways leading to increased formation of ROS/RNS.

3.4. Cell membrane and DNA damage following HPM exposure

The nucleus and membrane damage were evaluated using DAPI and PI fluorescence staining. The cell nucleus is represented by the blue fluorescence of DAPI. Only necrotic and dead cells exhibit PI fluorescence because PI is unable to enter live cells. The findings of DAPI and PI are given in Fig. 4A , B. No obvious changes were observed in MRC5 cells post-exposure (Fig. 4A). On the other hand, the DAPI staining of lung cancer H460 cells reveals nucleus damage following HPM exposure, particularly at 60 pulses. By increasing the number of pulses (15, 30, 45, and 60 pulses: 2.1 mJ/pulse), the PI staining also demonstrates that cell death increases, as indicated by the red color in Fig. 4B increasing in a dose-dependent manner. Fig. 4C shows the PI intensity in both lung normal MRC5 and lung cancer H460 cell lines. It is observed that the PI intensity increased dramatically only in the H460 cell line and increased in a dose-dependent manner, while the MRC5 remained unaffected.

3.5. HPM exposure inhibits cell migration in lung cancer

It is well known if cellular stress causes apoptosis/damage, they are able to migrate. We conducted a scratch assay to assess cell migration and verify whether H460 cells undergo damage from HPM exposure. Fig. 4D shows representative images taken at the indicated HPM pulse rates (15, 30, 45, and 60 pulses: 2.1 mJ/pulse) at the scratch area at 0 h and 24 h after exposure. Notably, the control group exhibited discernible migration, effectively bridging the scratch gap, and signifying cellular health. The HPM-treated group subjected to 30 or more pulses displayed a lack or no cell migration within 24 h, indicative of potential cellular damage by HPM (Fig. 4D). These results demonstrated that HPM exposure is effective at inducing cell damage or death, which is supported by the fact that lung cancer H460 cell migration was reduced.

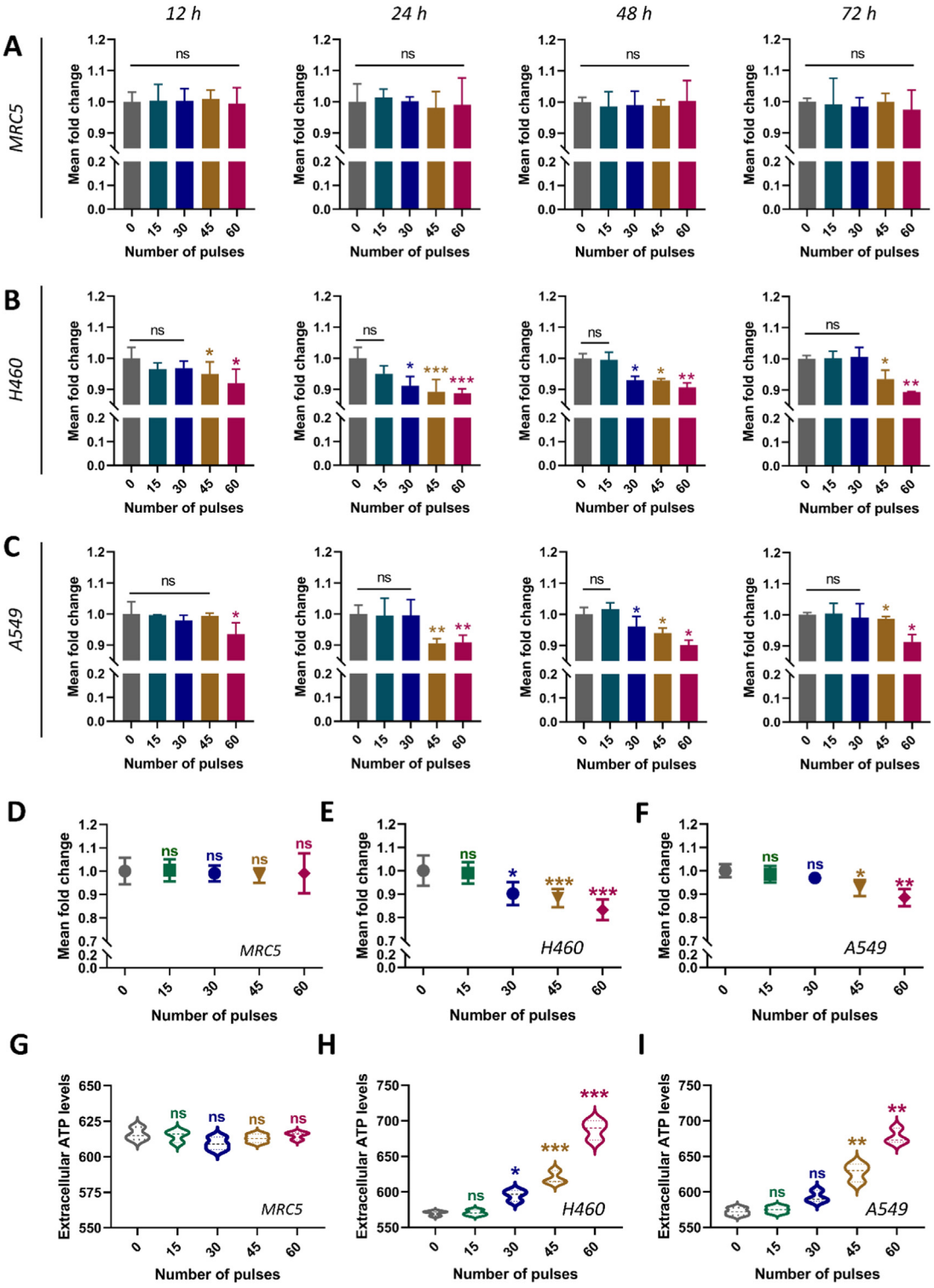

Fig. 2. The cell viability and ATP levels after exposure to HPM radiations. Pulsed HPM was applied to both healthy (MRC5) and cancerous (H460 and A549) lung cells (15, 30, 45, and 60 pulses; 2.1 mJ/pulse) and cell viability was evaluated at incubation periods 12, 24, 48, and 72 h after exposure. (A) The viability of lung normal MRC5 cells after exposure. At all chosen doses and incubation times, no significant reduction in the viability of MRC5 up to 60 pulses. (B) The survival of H460 lung cancer cells at 12, 24, 48, and 72 h following HPM exposure. The viability of lung cancer H460 cells was significantly reduced at 24 h after exposure to 45 and 60 HPM pulses and this effect persisted for 48 and 72 h of incubation. (C) The viability of lung cancer A549 cells post-exposure. The viability of A549 cells reduced dramatically at 45 and 60 pulses, 24 h after exposure. This effect continued after 48 and 72 h of incubation. (D)–(F) The intracellular ATP levels 24 h post-exposure in lung normal MRC5, and lung cancer H460, and A549 cells, respectively. No significant change in the ATP levels of MRC5 cells after HPM exposure while both cancers H460 and A549 showed a significant decrease. (G)–(I) Extracellular ATP levels in MRC5, H460, and A549 cells after HPM irradiation. The extracellular ATP levels elevated in both cancer cells while MRC5 remained unchanged after subjecting to HPM irradiation at selected doses. Microsoft Excel was used to calculate the significance (MS Office 365). Differences between treatment groups are denoted by $^{*}P < 0.05$, $^{**}P < 0.01$, and $^{***}P < 0.001$.

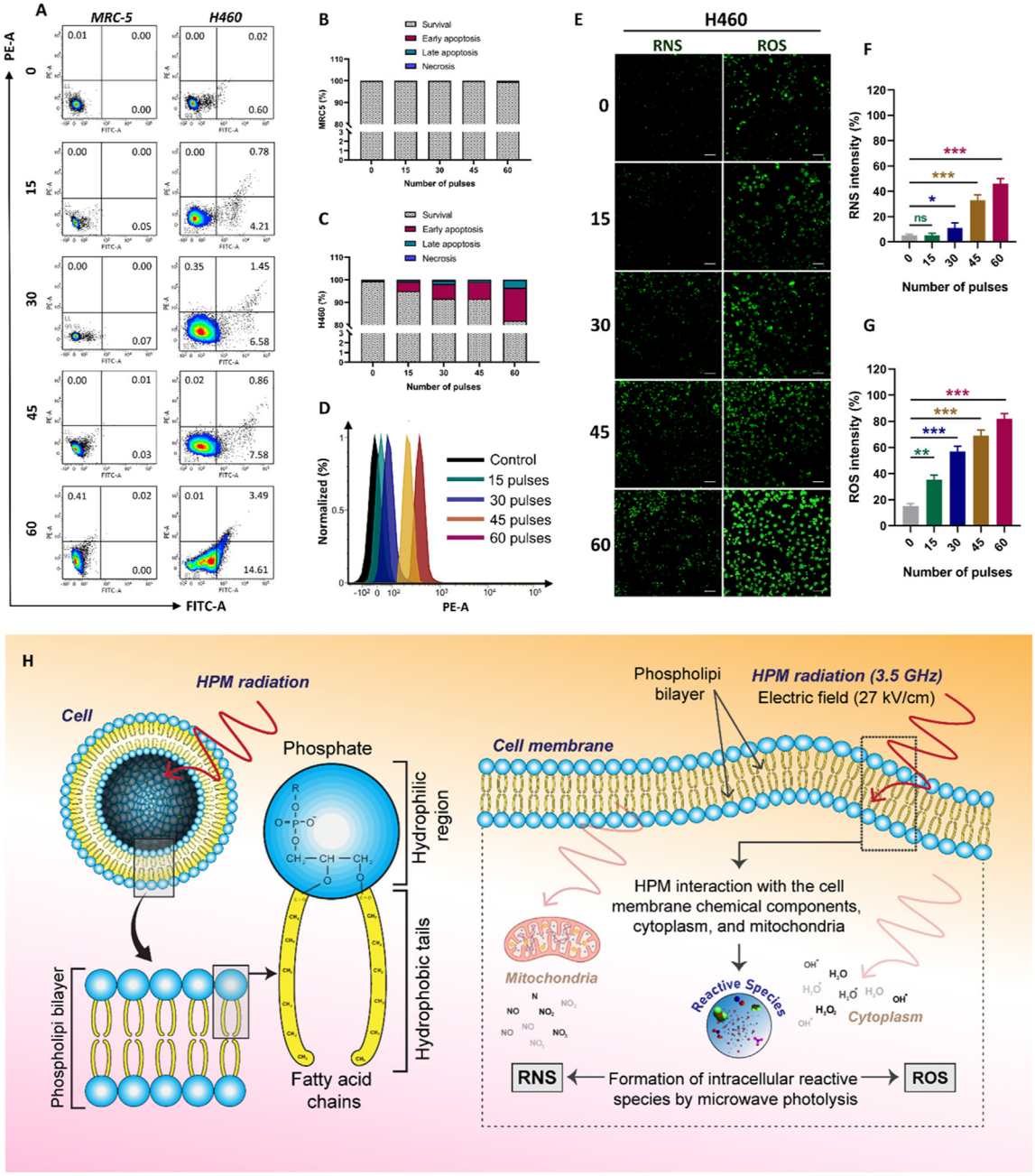

Fig. 3. The cell death analysis and intracellular ROS/RNS levels in lung normal MRC5 and lung cancer H460 cells, 24 h after HPM exposure at 15, 30, 45, and 60 pulses (2.1 mJ/pulse). (A) FACS scatter plots of cell populations displaying propidium iodide fluorescence, suggesting uptake in MRC5 and H460 cells ($n = 3$). The percentage of cell death in MRC5 and H460, including cell survival, early apoptosis, late apoptosis, and necrosis. (B) and (C) quantitative percentage of cell death in MRC5 and H460 24 h after HPM exposure. According to the findings, HPM pulses do not cause cell death in lung normal MRC5 cells at all selected doses. After being subjected to a maximum of 60 HPM pulses, over 99% of cells persisted within the cell survival quadrant. Comparing HPM-exposed groups to control groups, however, revealed a number of important differences in the populations of H460 cells. A dose-dependent pattern of cell death in H460 was seen. Maximum cell death was noted following HPM at 60 pulses. (D) Histogram analysis of PI staining in lung cancer cells (H460). When cells were exposed to HPM radiation pulses with 15, 30, 45, and 60 pulses, a shift in the curve was observed. (E) Intracellular ROS/RNS levels in H460, 24 h after HPM treatment (scale bar 100 μm). (F) and (G) relative intensity of RNS and ROS in the H460 cell line, respectively. HPM irradiation had significantly higher levels of RNS and ROS fluorescence levels in dose-dependent manner in H460 cells than in the untreated control group. (H) Possibility of the formation of intracellular ROS/RNS by HPM irradiation. When the electric field of $E = 27$ kV/cm produced by HPM interacted with cell membrane components (chemical composition), cytoplasm, and mitochondria, short and long-lived reactive species formed by the HPM.

3.6. Pulsed HPM irradiation elicits upregulation of apoptotic markers in H460 cells

Using quantitative PCR (qPCR), we examined the effects of 3.5 GHz pulsed HPM on the expression of genes related to apoptosis in lung cancer H460 and lung normal MRC5 cells. In order to determine whether 3.5 GHz HPM irradiation could cause the upregulation of expressions in lung normal MRC5 and lung cancer H460 cells, we performed experiments with various apoptosis-related molecular gene expressions. It is interesting to observe in Fig. 5A for MRC5, that the apoptosis-related

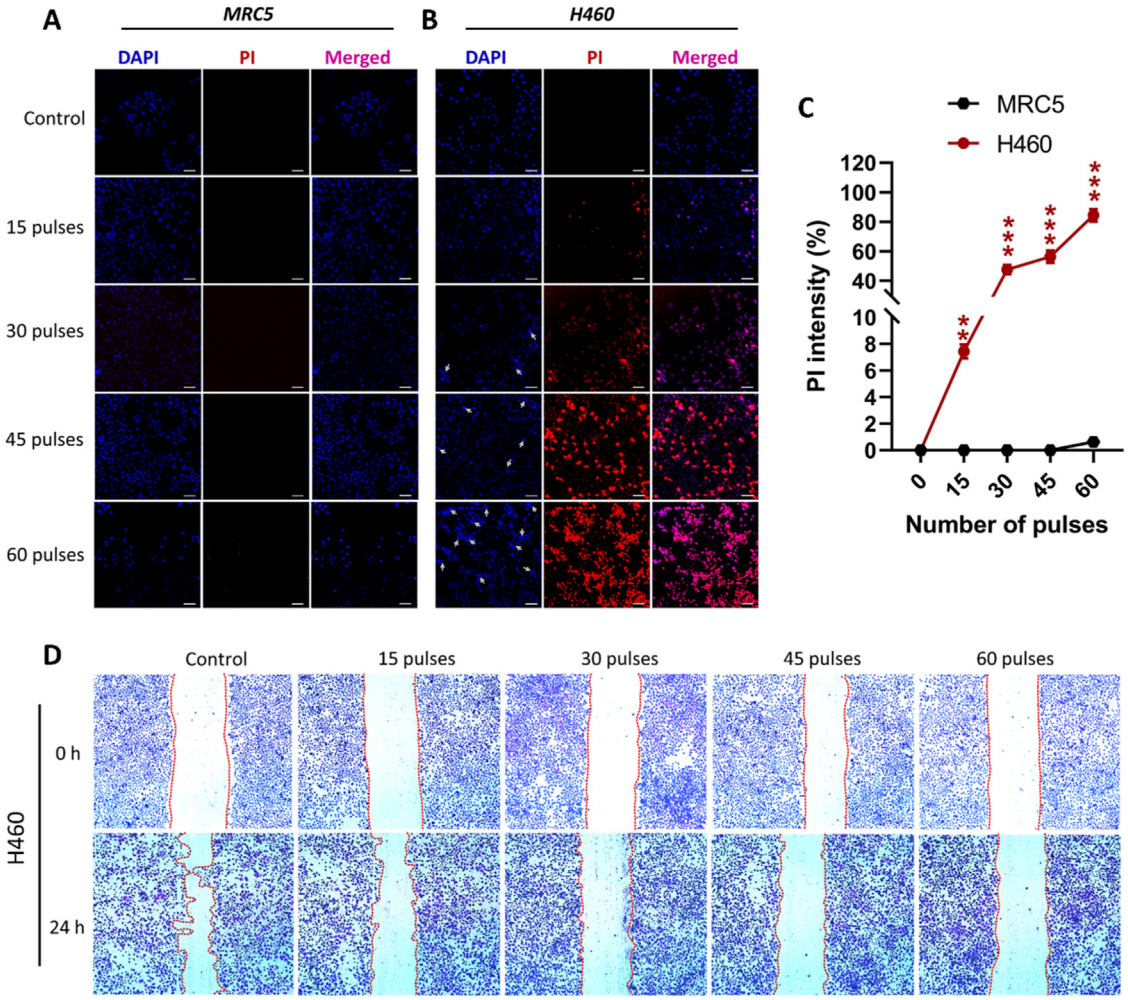

Fig. 4. DAPI, PI staining, and cell migration analysis. The cell nucleus was visualized by DAPI. Cell membrane damage was stained by PI. (A) and (B) shows the nucleus and membrane damage analysis by DAPI and PI staining in lung normal (MRC5) and cancer cells (H460) after HPM exposure, respectively. The nucleus of MRC5 is stained with DAPI, demonstrating that exposure to HPM does not harm the nuclei of healthy lung cells up to selected doses. Additionally, the PI staining shows no change after HPM exposure to selected doses. On the other hand, lung cancer H460 cells revealed nucleus damage following HPM exposure, particularly at 45 and 60 pulses. By increasing the number of pulses (15, 30, 45, and 60 pulses: 2.1 mJ/pulse), the PI staining also demonstrates that cell death increases, as indicated by the red color increasing in a dose-dependent manner (scale bar: 100 μm). (C) Quantitively percentage of PI fluorescent after selected HPM pulses. (D) Lung cancer cells (H460) migration after HPM treatment at 15, 30, 45, and 60 pulses immediately after exposure (0 h) and after 24 h. When H460 cells were treated with HPM pulses, there was a significant reduction in the migration of H460 cells which confirms the cell damage or death, as evidenced by the images of gap closure in the control and HPM-treated cells. These results demonstrated that HPM exposure is effective at inducing cell damage or death, which is supported by the fact that lung cancer H460 cell migration was reduced.

markers remained unchanged or unaffected after HPM exposure. The lung cancer H460 cell, on the other hand, experienced a significant fold increase in apoptotic genes following exposure to HPM, as demonstrated in Fig. 5B. After HPM exposure to 30, 45, and 60 pulses, there was a significant increase in the expression of ATR, ATM, Chk1, and Chk2 in lung cancer H460 cells, and the increase was seen in a dose-dependent manner only in H460 cells while they remained unchanged in MRC5 cells. This increase in markers shows that HPM radiation caused DNA damage only in H460 lung cancer cells. By analyzing the expression of BRCA1 and BRCA2, we have further looked into identifying DNA repair. Up to the 30 HPM pulses, the expression of BRCA1 and BRCA2 was observed to be unchanged, and at 45 and 60 pulses, the expression was seen to decrease (Fig. 5B). The chosen HPM pulses did not affect lung normal MRC5 cells. The subsequent activation of ATM/ATR led to the activation of p53 in H460 cells. At 30, 45, and 60 pulses of HPM, the expression of P53 significantly increased in dose-dependent manners.

Additionally, after HPM in H460 cells, especially at 60 pulses, a cell cycle arrest marker called CDC25c was observed to be elevated. The role of P53 activation for apoptosis was confirmed by the upregulation of the expressions of Bax and Bak. After being exposed to HPM radiation, the levels of caspase-3 and caspase-8 also increased in H460 cells in a dose-dependent manner, but they remained unchanged in MRC5 (Fig. 5A, B). The levels of Bcl2 activity in lung normal MRC5 cells did not change in response to the HPM pulses (15, 30, 45, and 60), but the expression of Bcl2 in lung cancer H460 cells was markedly downregulated after exposure. Fas expression levels in normal lung MRC5 cells have not changed noticeably, but it is upregulated in H460 cells, where it also increased in a dose-dependent manner. The EGF, which is typically linked to cell proliferation, was not significantly influenced after HPM exposure in either MRC5 or H460 cells. Similar to this, the expression of TRAIL was unaffected in normal and cancerous lung cells exposed to HPM. The final indicator that the cell is about to undergo apoptosis is the PARP. It has been noted that the expression levels of PARP have only increased

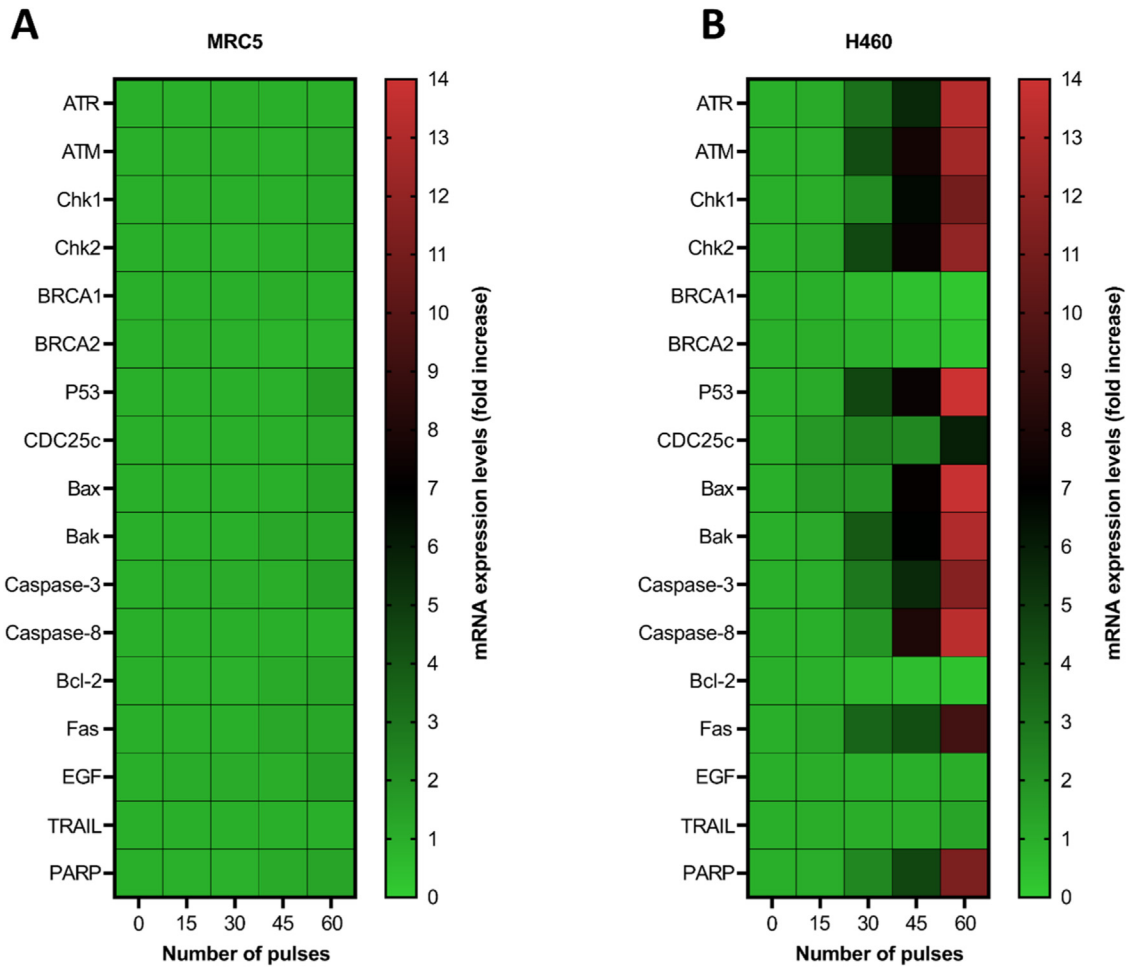

Fig. 5. Molecular analysis in MRC5 and H460, 24 h after HPM exposure. (A) The molecular analysis of the MRC5 cells and (B) lung cancer H460 cells line after irradiation at selected dosage. It is interesting to observe for MRC5, the apoptosis-related markers remained unchanged or unaffected after HPM exposure at 15, 30, 45, and 60 pulses (2.1 mJ/pulse). The lung cancer H460 cell, on the other hand, experienced a significant fold increase in apoptotic genes following exposure to HPM. After HPM exposure to 30, 45, and 60 pulses, there was a significant increase in the expression of ATR, ATM, Chk1, and Chk2 in lung cancer H460 cells, and the increase was seen in a dose-dependent manner only in H460 cells while they remained unchanged in MRC5 cells. This increase in markers shows that HPM radiation caused DNA damage only in H460 lung cancer cells. The expressions of BRCA1 and BRCA2 at 45 and 60 pulses were seen to decrease. The subsequent activation of ATM/ATR led to the activation of p53 in H460 cells. At 30, 45, and 60 pulses of HPM, the expression of P53 significantly increased in dose-dependent manners. Additionally, after HPM in H460 cells, especially at 60 pulses, a cell cycle arrest marker called CDC25c was observed to be elevated. The role of P53 activation for apoptosis was confirmed by the upregulation of the expressions of Bax and Bak. After being exposed to HPM radiation, the levels of caspase-3 and caspase-8 also increased in H460 cells in a dose-dependent manner. The levels of Bcl2 in lung cancer H460 cells were markedly downregulated after exposure. Fas expression levels in normal lung MRC5 cells have not changed noticeably, but it is upregulated in H460 cells, where it also increased in a dose-dependent manner. The EGF, which is typically linked to cell proliferation, was not significantly influenced after HPM exposure in either MRC5 or H460 cells. Similar to this, the expression of TRAIL was unaffected in both cells after treatment. The final indicator that the cell is about to undergo apoptosis is the PARP which is upregulated in H460 after exposure.

in lung cancer H460 cells, whereas they were maintained (no change) in normal MRC5 cells (Fig. 5A, B).

3.7. Protein analysis validates DNA damage and apoptosis triggered by HPM exposure

In addition, protein analysis was done by western blot to support the results mentioned above. We have observed from a prior experiment (Fig. 6A, B) that the lung normal MRC5 cells have no effect after HPM exposure. Only the lung cancer H460 cells displayed considerable alteration, with the maximum effect being seen at 60 pulses. We have selected the lung cancer H460 cell and 60 pulses as HPM treatment for further analysis. Using 60 pulses (2.1 mJ/pulse) of radiation exposure on the lung cancer H460, the protein analysis was carried out. The results obtained from the protein analysis are shown in Fig. 6A, and the relative band intensity is in Fig. 6B. First, we noticed that exposure to 3.5 GHz HPM caused DNA damage and P53 activation, which led to cell apoptosis. It is noticed that the protein expression level in P53 increased in H460 cells after exposure to HPM radiations at 60 pulses. The activation of P53 confirms the DNA damage after HPM exposure [29]. The P53 protein analysis results are consistent with the findings of the molecular analysis (Fig. 5B). Further, we looked into the protein expression of Bax, which also increased after HPM treatment, to confirm that P53 activation resulted in cell apoptosis [30]. It is noticed that the band intensity of the P53, caspase-3, Bax, Apoptotic protease activating factor (APAF), and Cleaved PARP was increased after HPM exposure to 60 pulses in H460 NSCLC. Following HPM therapy, cancer cells are depicted in Fig. 6A progressing through the P53-activated apoptotic pathway. The band intensity is higher in the 60-pulses group compared to the control group (Fig. 6B). These results show that H460 cells produce specific ROS/RNS in response to HPM radiation, which results in DNA damage. Additionally, we noticed that cells are more vulnerable to apoptosis brought on by various stimuli when the intrinsic pathway is overexpressed (Bax and cytochrome *c*). Notably, the activation of P53

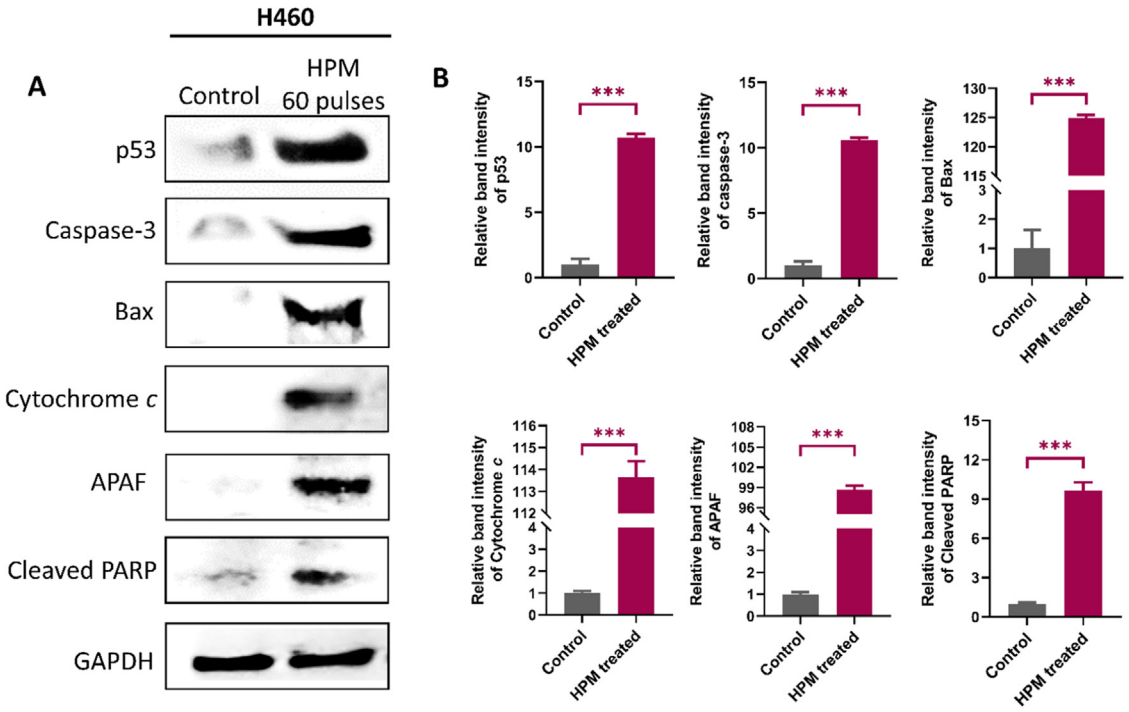

Fig. 6. Protein analysis of lung cancer H460 cells by using western blot. (A) Protein analysis of NSCLC H460 after HPM exposure of 60 pulses. The protein expression and activation of p53 in H460 cells 24 h after HPM exposure at 60 pulses. It is noticed that the protein expression level in P53 increased in H460 cells after irradiation. The increased protein expression of Caspase-3, Bax, Cytochrome c, APAF, and cleaved PARP after HPM irradiation confirms that P53 activation resulted in cell apoptosis. (H) The relative band intensity.

after HPM exposure probably aids in the activation of an intrinsic pathway to induce cell death.

3.8. ROS/RNS production triggered by pulsed HPM primarily responsible for cellular effects

The NAC is a scavenger of the reactive species (both ROS/RNS, mainly ROS) [31], which is used to determine whether the induced reactive species by HPM irradiation are primarily accountable for the various effects in NSCLC. First, different concentrations of NAC were taken to observe the cell viability of MRC5 and H460 to observe its acceptable concentration, and results are displayed in Fig. 7A, B. NAC was used at a concentration of 5 mM for the additional study because it has no cytotoxic effects on cells. Additionally, it is verified that, following HPM exposure, NAC (5 mM) notably managed to decrease ROS/RNS levels, taking them to a non-significant level (Fig. 7C, D). Interestingly, we observed a recovery in the viability of H460 cells (Fig. S10) after subjecting the HPM exposure to NAC. Furthermore, a decrease in cell death rate following the administration of NAC was also observed (Fig. 7E, F). The percentage of H460 cell death (comprising early apoptosis, late apoptosis, and necrosis) was originally 18.11% without NAC following 60 HPM pulses, which significantly reduced to a negligible 1.08% after NAC treatment (Fig. 7F). This substantial reduction underscores the pivotal role of elevated ROS/RNS levels in H460 cell death triggered by HPM exposure. Moreover, the markers associated with DNA damage and apoptosis exhibited dramatic downregulation subsequent to the use of NAC, providing a conclusive indication that ROS/RNS plays a pivotal role in driving cellular effects (Fig. 7G).

We hypothesize that among the array of various RNS, nitric oxide (NO) emerges as a highly reactive and pivotal contributor to cellular effects. Notably, NO species can undergo subsequent conversion into more stable and long-lived species collectively referred to as NO_x. Our objective is to hinder the formation of NO species, which predominantly contributes to the inhibition or neutralization of RNS species, through the use of a CPTIO inhibitor. We are able to recognize the individual roles of NO species in the induction of cellular effects owing to the strategic utilization of a CPTIO inhibitor. Different concentrations of CPTIO inhibitor were taken to observe the cell viability of MRC5 and H460 to observe its acceptable concentration and results are displayed in Fig. 7H and I. Both the direct formation of stable NO_x species and the initial generation of NO followed by further reactions to produce NO_x are plausible scenarios depending on the experimental conditions. In this work, we have identified a noteworthy decrease in the concentration of NO_x in RPMI upon the application of the CPTIO inhibitor with HPM irradiation (Fig. 7J). This outcome provides compelling evidence that the primary sequence of reactions involves the generation of NO species first, which subsequently leads to the formation of NO_x. The ROS (H_2O_2) levels appeared to be unchanged after subjecting the CPTIO inhibitor (Fig. 7K). Interestingly, we observed a slight recovery in the viability of H460 cells (Fig. S11) after subjecting the HPM exposure to a CPTIO-inhibitor compared with the HPM-exposed group without CPTIO. Furthermore, a small decrease in cell death rate following the administration of CPTIO was also observed (Fig. 7L, M). The percentage of H460 cell death (comprising early apoptosis, late apoptosis, and necrosis) was originally 18.11% without CPTIO following 60 HPM pulses, which reduced to 14.11% after CPTIO treatment (Fig. 7M). These findings highlight that the 4% cell death observed in H460 cells can be attributed to the presence of NO species. Moreover, this suggests that the primary driving species behind the cell death process is ROS, with RNS also exerting a contributing influence. Despite the use of the CPTIO inhibitor, markers associated with DNA damage and apoptosis displayed reduced but still significant expression levels (Fig. 7M), supporting the key role of ROS in cellular effects, with NO species as the contributing factor. Neutralizing reactive species with NAC scavenger and CPTIO inhibitors led to a marked decrease in the expressions of markers associated with apoptosis and DNA damage. These findings strongly support that the effects observed after HPM irradiation are primarily mediated by ROS/RNS.

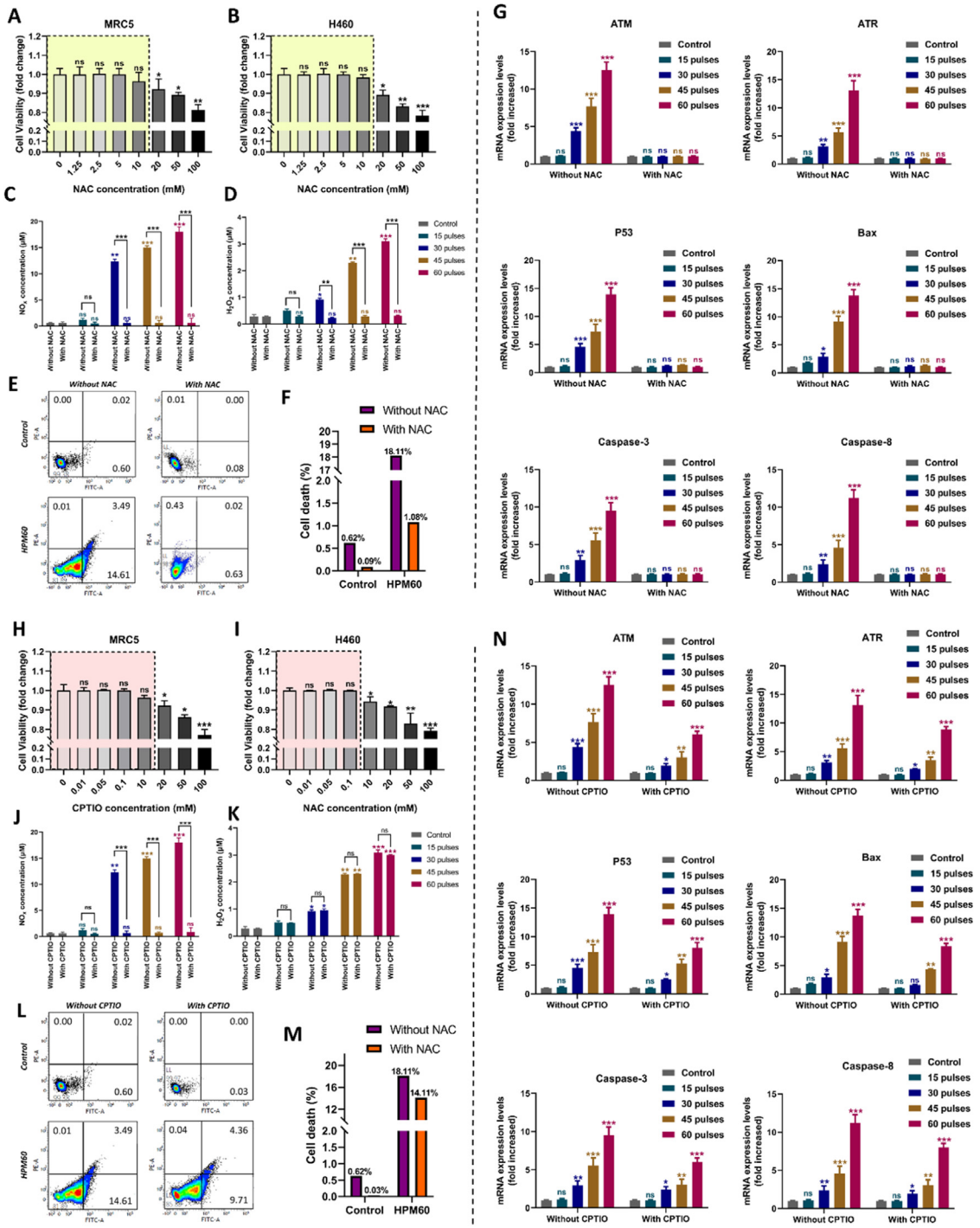

Fig. 7. The role of reactive species in inducing cellular effects, 24 h after HPM irradiation. (A)–(G) The use of NAC (5 mM) scavenger to confirm the role of ROS/RNS (mainly ROS) in cell death and its related effects. The cell viability of lung normal (A) MRC5 and NSCLC (B) H460 cells with the different concentrations of NAC scavenger. The concentrations of (C) NO_x and (D) H_2O_2 in cell culture media without and with NAC (5 mM), were measured immediately after HPM exposure. The amount of ROS/RNS in RPMI significantly reduced and became non-significant after using 5 mM NAC. (E) The analysis of cell death in H460 cells exposed to 60 HPM pulses, both with and without using NAC scavenger. A significant decrease in cell death rates upon the application of the NAC scavenger was observed. (F) Without NAC scavenger cell death rate is 18.11% at 60 HPM pulses which is reduced to a negligible 1.08%. (G) The PCR analysis of DNA damage and cell death markers (ATR, ATM, P53, Bax, Caspase-3, Caspase-8.) without and with using NAC scavenger. The expressions of the genes related to DNA damage and cell death significantly decreased and became nonsignificant after using NAC which confirms that ROS/RNS are mainly responsible for cellular effects. (H)–(N) The use of CPTIO (0.1 mM) inhibitor to confirm the role of NO species in cell death and its related effects. The cell viability of lung normal (H) MRC5 and (I) H460 cells with the different concentrations of CPTIO inhibitor. The concentrations of (J) NO_x and (K) H_2O_2 in cell culture media without and with CPTIO, were measured immediately after HPM exposure. The amount of NO_x in cell culture media was significantly reduced by using CPTIO while H_2O_2 remained unchanged. Notably, NO species can undergo subsequent conversion into more stable and long-lived species collectively referred to as NO_x. (L) The analysis of cell death in H460 cells exposed to 60 HPM pulses, both with and without using CPTIO. (M) A 4% decrease in cell death rates upon the application of the CPTIO was observed in H460 cells. (N) The PCR analysis of DNA damage and cell death markers (ATR, ATM, P53, Bax, Caspase-3, Caspase-8.) without and with using CPTIO inhibitor. Cell death rates, expressions of DNA damage markers, and apoptosis all slightly decreased but remained statistically significant even in the presence of the CPTIO inhibitor. This emphasizes that ROS plays a major role in cellular effects, with NO species possibly playing a supporting role.

4. Discussion

The biological effects of microwaves can be significantly influenced by their physical properties, such as electric field intensity, oscillating frequency, and exposure time [32–35]. Here, we found that the temperature and pH of the cell medium did not significantly change after HPM irradiation (Fig. 1G, H), suggesting that the effect on the cells is not thermal. Before diving into the biological effects of pulsed HPM, it is essential to consider its physical characteristics, including power, frequency, pulse duration, emission mode, especially the electric field strength at the sample position, and EM energy delivered to cells. We have carefully examined the characteristics of HPM (Fig. 1B–1D) and its impact on the media for cell culture (Fig. 2I–2L). Further additional details of HPM were given in supporting information in Figs. S1 to S4. It is interesting to note that the concentrations of NO_x and H_2O_2 levels inside RPMI increase in a dose-dependent manner after being exposed to HPM (Fig. 2I, J). These species known as extracellular ROS/RNS later diffused inside the cells and caused potential biological effects.

The possible mechanism of the formations of these extracellular ROS/RNS (inside RPMI) is important to discuss. The interaction between the ambient air gasses and the electric field produced by the pulsed HPM can be used to explain how these reactive species are produced inside RPMI. The ambient media atmosphere contains water vapor (H_2O), molecular oxygen (O_2), and molecular nitrogen (N_2). At the air-liquid interface, an electric field of about 27 kV/cm of HPM interacts with the molecules of nitrogen and oxygen and transforms them into their atomic species of oxygen and nitrogen. These could also mix to produce NO_x, which would then be incorporated into the liquid. Both NO_x and H_2O_2 species were found to be increased inside media in which the NO_x concentration is dominant (Fig. 2I, J). HPM can also affect gene expression and a number of biological processes, including apoptosis, autophagy, and cell-cycle control [36]. The effect of pulsed HPM on cancer cells was investigated in the previous reports [37–39]. The effect of HPM radiation on brain cancer cells was also investigated and it is observed that RONS production in response to HPM pulses is mainly responsible for cell apoptosis and associated effects on cells [23]. The levels of intracellular ROS/RNS were also elevated in H460 cells as a result of the strong electric field provided by pulsed HPM (Fig. 3E). Studies have suggested that exposure to microwave radiation can increase ROS production in cells [23,37,40]. However, the exact mechanism by which microwave radiation induces ROS/RNS production inside cells is not fully understood. In this work, we have explained the possible mechanism of the formation of intracellular ROS/RNS. The enhancement in intracellular ROS/RNS levels can be explained by the microwave as shown schematically in Fig. 3H. When the electric field $E = 27$ kV/cm produced by HPM interact with cell membrane components (chemical composition), cytoplasm, and mitochondria, short lived ROS species such as H_2^*, OH^-, H^+, $OH^\bullet$ and long-lived species, H_2O_2 formed inside the cell by the HPM [41]. Similarly, the RNS species NO, NO^-, NO_2^-, and NO_3 formed. The potential mechanism of the formation of long and short lived ROS can be explained as follows [41,42]:

$$E + H_2O \rightarrow H_2O^* \quad (1)$$

$$E + H_2O^* \rightarrow OH^\bullet + H^\bullet \text{ or } O + 2H \quad (2)$$

$$OH^\bullet + OH^\bullet \rightarrow H_2O_2 \text{ or } H_2O + O \quad (3)$$

$$H_2O^* \rightarrow OH^- + H^+ \quad (4)$$

$$OH^- + OH^- \rightarrow H_2O_2 + 2e^- \quad (5)$$

Similarly, the short and long-lived RNS can be formed as [43]:

$$E + N + O \rightarrow NO^\bullet \quad (6)$$

$$NO^\bullet + NO^\bullet \rightarrow N^\bullet + NO_2 \quad (7)$$

$$E + NO^\bullet + NO^- \rightarrow NO_2^- \quad (8)$$

$$E + NO^\bullet + NO_2^- \rightarrow NO_3^- \quad (9)$$

These short-lived and long-lived intracellular ROS/RNS played important roles in the activation of pathways that led to physiological changes and cell apoptosis. Interestingly, the intracellular ROS/RNS content in MRC5 cells was non-significant compared to control up to 45 pulses, but there was a slight increase at 60 pulses only, suggesting that this small amount of increase might not be harmful to normal cells (Fig. S9). In NSCLC (H460), the intracellular ROS/RNS concentration is noticeably higher, and these species are mainly responsible for the process of cell apoptosis (Fig. 7).

In response to genotoxic stress, the P53 (tumor suppressor gene), a sequence-specific transcription factor, activates the expression of genes involved in promoting cell growth arrest or cell death [44]. In this work, the ATR/ATM, Chk1/Chk2 pathway activated only in lung cancer H460 cells which confirms the DNA damage after HPM exposure. After HPM irradiation, we hypothesize that the long-lived and short-lived intracellular ROS/RNS caused DNA damage, P53 stimulation, and activation of the intrinsic pathway to induce cell death in NSCLC (Figs. 5–7). We can demonstrate that the HPM exposure does not have an immediate impact because no noticeable effects were observed at 12 h after the exposure. A significant decline in viabilities and ATP was noted at 24 h in both NSCLC A549 and H460 (Fig. 2). According to the findings, both of the NSCLCs (H460 and A549) that were being examined underwent apoptosis after being exposed to HPM radiation. It is widely acknowledged that mitochondria play a significant part in the supervision of apoptosis. After HPM treatment in H460 cells, the levels of Bax, Bak, and cytochrome *c* significantly increased (Fig. 5). One such possibility is that the intrinsic pathway is activated and apoptosis is started as a result of HPM-induced ROS/RNS generation. Despite the fact that the mechanisms controlling the permeabilization of the outer mitochondrial membrane and the release of intermembrane space proteins are still debatable, the release of cytochrome *c* from mitochondria is a crucial first step in the apoptotic process [45]. Later, the expression of the ATR/ATM, Chk1/Chk2 pathway allowed us to further confirm the DNA damage following exposure to the HPM (Fig. 5). The findings show that HPM exposure causes DNA damage and activates the mitochondrial intrinsic pathway. Both work synergistically to induce apoptosis in H460 cells. It is important to notice that, when NAC was applied to scavenge the ROS/RNS, the decrease in cell viability and cell death after HPM irradiation became non-significant (Fig. 7A–7G). These results help to confirm that the activation of marker related to DNA damage and cell apoptosis, only upregulated in the presence of the ROS/RNS as shown in Fig. 7G. We seek to reduce the production of NO species, a key precursor of NO_x species (as shown in Eqs. 6 to 9), by using the CPTIO inhibitor. This strategic approach provides us a thorough understanding of the unique roles that NO species play in cellular effects. Our results reveal a slight decrease in cell death rates and expressions of genes related to DNA damage and apoptosis but remained significant. The result after CPTIO treatment indicates that NO species only account for 4% of cell death in H460 cells while ROS are mainly responsible for inducing cell death (Fig. 7).

Following HPM irradiation of NSCLC, Fig. 8 depicts a potential mechanism for cell apoptosis (H460). HPM irradiation causes DNA damage in NSCLC, as evidenced by the increased expression of the ATR/ATM and Chk1/Chk2 markers. Further, it leads to the upregulation of P53, Bax, and the downregulation of Bcl-2. The release of cytochrome *c* and

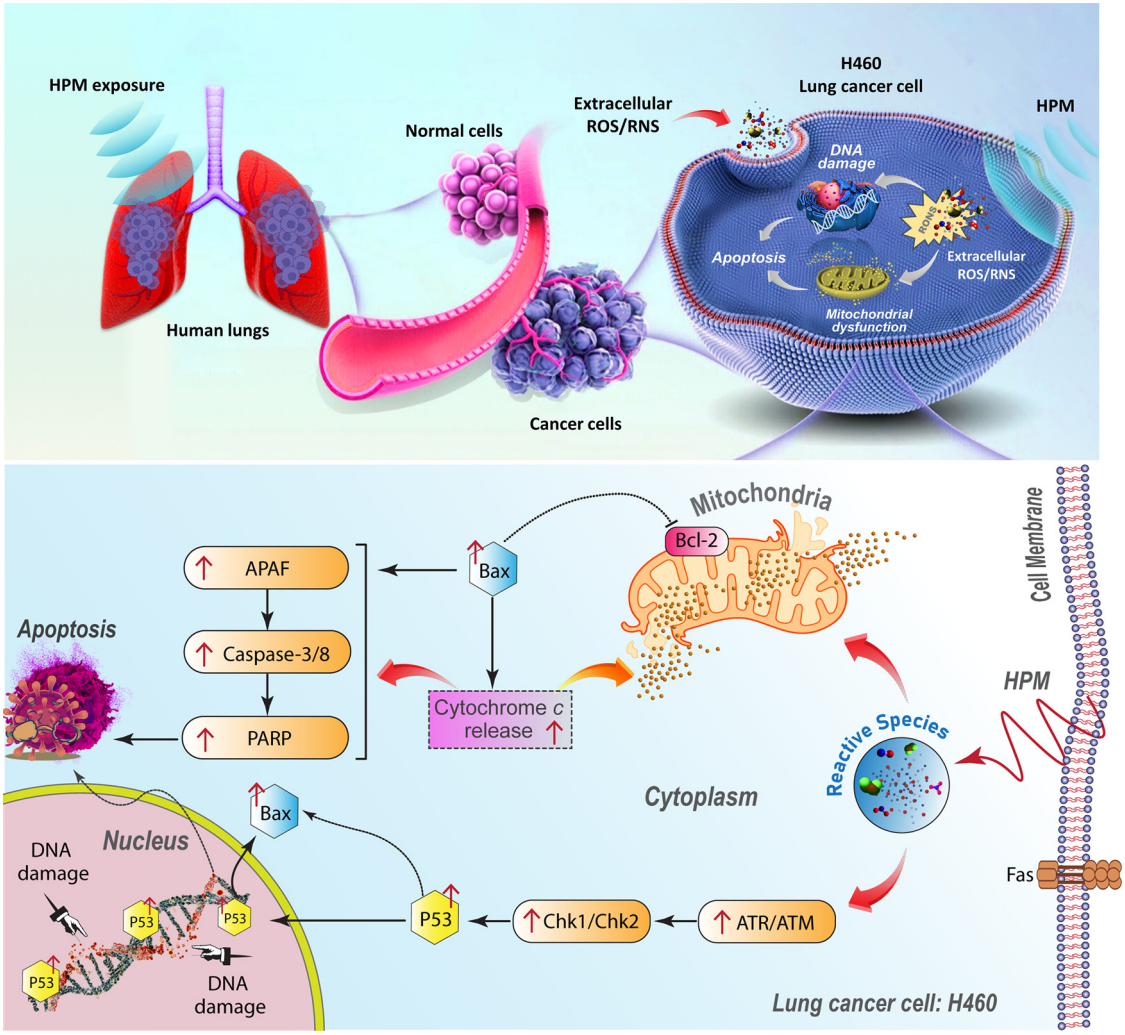

Fig. 8. The possible mechanism involved for cell apoptosis in NSCLC (H460) after HPM irradiation. Exposure to a specific amount of HPM radiation initiates the generation of ROS/RNS, a process critical for potential cellular effects. ROS/RNS are initially induced within the cell culture medium (RPMI), referred to as extracellular ROS/RNS. Subsequently, they diffuse into the cell due to membrane damage, membrane opening, or electroporation caused by a strong electric field of HPM. Moreover, ROS/RNS can also form within the cell itself when HPM interacts with the chemical components of the cell membrane, mitochondria, and the cytoplasmic region, or the activation of a pathway to induce more ROS/RNS. The diffusion of these extracellular ROS/RNS into the cell and the in-situ formation of intracellular ROS/RNS both contribute significantly to an elevated level of these reactive species within the cell. These species are primarily known to induce DNA damage, as they activate pathways involving ATR/ATM and Chk1/Chk2, ultimately leading to the activation of the p53 protein. Furthermore, p53 plays a role in downregulating the expression of Bcl-2 while simultaneously upregulating the expression of Bax. Following HPM irradiation, there was an observed increase in the release of cytochrome *c*, which triggered the activation of APAF, Caspase 3/8, and PARP to promote apoptosis in lung cancer H460 cells.

activation of the caspase cascade increased significantly only in NSCLC (H460) after HPM treatment. Furthermore, the activation of APAF and PARP shows that after being exposed to HPM radiation, the cell enters an apoptotic state [46]. We discovered throughout the experiments that the HPM radiation at particular doses (15, 30, 45, and 60 pulses: 2.1 mJ/pulse) had no effect on the lung normal MRC5 cells. Only NSCLC (H460 and A549) exhibits appreciable changes after being exposed to HPM. It is safe to say that, at specific doses, HPM irradiation may result in DNA damage, mitochondrial ROS/RNS, the release of cytochrome *c*, and activation of P53 and Bax, which in turn activates caspase-3 in both NSCLC A549 and H460.

Skin depth is a term used to describe the depth at which EM waves penetrate into a conducting body [47]. It is the distance from the surface at which the amplitude of an EM wave is reduced to $e^{-1} = 0.37$ of its original value. For therapeutic applications of HPM, the skin depth was also calculated by using the formula given as

$$\delta = \frac{2}{\sqrt{\omega g \mu}} \tag{10}$$

where $\omega = 2\pi f$, f is the frequency of HPM. The μ indicates the magnetic permeability and $g = 0.3$ S/m is the conductivity. In this work, the skin penetration depth was calculated as $\delta = 30$ mm. Since depending on individuals, the average distance between the lungs and the outer skin is between 10 and 20 mm, the skin depth ($\delta \cong 30$ mm) suggests that the HPM technique is applicable for practical use. Furthermore, it is also important to note that the skin depth depends on the frequency of HPM which can be adjusted according to the requirements.

The differences in cytotoxicity between cancer and normal cells in response to a particular dose or stimulus can be attributed to a range of factors, including genetic mutations, metabolic distinctions, influences from the microenvironment, and different ROS/RNS levels [48–50]. An example was found in a study investigating the cytotoxicity of paclitaxel, revealing a more pronounced effect on neoplastic cells compared to normal cells, indicating a cell type-dependent response. It is also reported that the cancer cells might not have their normal capacity for bioenergetic compensation, which makes them more vulnerable to certain stimuli [51]. A further layer of complexity results from the function

of cancer-associated fibroblasts in regulating the survival and growth of cancer cells, emphasizing the complex interactions between various cell types in the tumor microenvironment. This specificity occurred due to the inherent or naturally different properties of cancer and normal cells. Cancer cells usually exhibit higher levels of ROS/RNS due to their higher metabolic activity compared to normal cells [52,53]. Upon external stimuli (such as HPM exposure) the concentration of ROS/RNS in cancer cells reaches to substantial level to cause cell damage/death in lower HPM doses compared to normal cells. Hence, the killing effects on normal and cancer cells manifest within different dose ranges.

HPM constitutes non-ionizing radiation, which implies that it does not cause direct damage to cells. Instead, it operates through indirect mechanisms such as the formation of ROS/RNS. In this work, the different impacts of HPM on normal and cancer cells can be attributed to the ROS/RNS levels [54]. The heightened metabolic activity inherent in cancer cells results in higher intracellular ROS/RNS levels compared to normal cells [53,55]. Upon exposure to HPM irradiation, a significant increase in ROS/RNS levels is observed in cancer cells (Fig. 3E–3G). These ROS/RNS mainly contribute to the observed decrease in cell viability (Fig. 7). Conversely, when subjecting MRC5 lung normal cells to HPM, a small increase in ROS levels is noted, with RNS levels showing no significant change from the control group up to 60 pulses (Fig. S9). We have confirmed that the ROS/RNS are predominantly accountable for the outcomes observed in this study, as demonstrated by the application of the NAC scavenger and CPTIO inhibitor (Fig. 7). This study may serve as a valuable foundation for future research endeavors. Given that the electric field of pulsed HPM is strong enough to induce electroporation, this capability holds great promise for our forthcoming investigations focused on drug delivery.

HPM exposure presents a distinctive approach to cancer treatment, offering advantages that differentiate it from other techniques such as photothermal [56], magnetothermal [57], and ultrasonic methods [58]. One notable advantage of HPM is its non-invasive nature, as it doesn't rely on physical contact with the tumor site. Unlike photothermal therapy, which requires the precise targeting of light-absorbing agents, or magnetothermal therapy, HPM delivers energy remotely, potentially minimizing damage to surrounding healthy tissues. Additionally, the high electric field (27 kV/cm) of nanosecond pulsed HPM possesses the potential to induce electroporation, a phenomenon that could prove beneficial for drug delivery purposes [59]. Each method comes with its unique set of advantages and limitations. It is crucial to emphasize that the exploration of HPM in cancer research is in its early stages and requires thorough investigation in the future.

5. Conclusion

In this work, a strong electric field (27 kV/cm) by pulsed HPM primarily generates ROS/RNS, which alters NSCLC cell viability, mitochondrial activity, and cell death rates. Interestingly, only NSCLC (H460 and A549) were found to be impacted by HPM pulses, while lung normal MRC5 cells remained unaffected up to 60 pulses. These changes may have occurred as a result of DNA damage, as indicated by the upregulation of ATR/ATM, Chk1/Chk2, and P53, as well as a rise in the expression of apoptotic markers (Bax, Bak, Caspase-8, Caspase-3, and PARP). Additionally, it was found that HPM inhibited cell migration after exposure. NAC scavenger and CPTIO confirm that the reactive species are accountable for cellular effects. Interestingly, a recovery in the viability of H460 cells and a decrease in cell death rate was observed following the administration of NAC. Moreover, the markers associated with DNA damage and apoptosis exhibited dramatic downregulation with the use of NAC, providing conclusive evidence that reactive species play a pivotal role in driving cellular effects. Despite the CPTIO-inhibitor (NO inhibitor), cell death rates, markers related to DNA damage, and apoptosis showed lower but still significant expression levels. This reinforces the main role of ROS in cellular effects, with NO species possibly playing a contributing role. These findings support the cellular mechanisms underlying NSCLC HPM-induced cell death. The skin depth ($\delta \cong 30$ mm) suggests that the HPM technique is applicable for real use. This technique offers significant advantages over conventional methods by enabling non-surgical cancer treatment. Moreover, this technique has the potential to serve as an adjunct to non-surgical methods in cancer therapy. The findings of this study may be helpful for future research and in advancing therapeutic approaches to treating NSCLC.

Data availability statement

The corresponding author will provide the original data used to support the findings of this study upon reasonable request.

CRediT authorship contribution statement

Juie Nahushkumar Rana: Writing – review & editing, Writing – original draft, Visualization, Validation, Software, Methodology, Investigation, Formal analysis, Data curation, Conceptualization. **Sohail Mumtaz:** Writing – review & editing, Writing – original draft, Validation, Software, Methodology, Formal analysis, Data curation, Conceptualization. **Ihn Han:** Supervision, Conceptualization. **Eun Ha Choi:** Writing – review & editing, Supervision, Resources, Project administration, Funding acquisition, Conceptualization.

Declaration of competing interest

The authors declare that they have no conflicts of interest in this work.

Acknowledgments

This work was supported by the National Research Foundation of Korea (NRF) with grants funded by the Korean government (MIST) (NRF-2022R1A2C1004257, NRF-2021R1A6A1A03038785), and Kwangwoon University, Seoul, Korea, 2023.

Supplementary materials

Supplementary material associated with this article can be found, in the online version, at doi:10.1016/j.fmre.2024.02.001.

References

[1] S. Mumtaz, J.N. Rana, E.H. Choi, et al., Microwave radiation and the brain: mechanisms, current status, and future prospects, Int. J. Mol. Sci. 23 (2022), doi:10.3390/ijms23169288.
[2] R. Chandra, H. Zhou, I. Balasingham, et al., On the opportunities and challenges in microwave medical sensing and imaging, IEEE Trans. Biomed. Eng. 62 (2015) 1667–1682.
[3] E.J. Bond, X. Li, S.C. Hagness, et al., Microwave imaging via space-time beamforming for early detection of breast cancer, IEEE Trans. Antennas Propag. 51 (2003) 1690–1705.
[4] E.C. Fear, X. Li, S.C. Hagness, et al., Confocal microwave imaging for breast cancer detection: localization of tumors in three dimensions, IEEE Trans. Biomed. Eng. 49 (2002) 812–822.
[5] A. Fhager, S. Candefjord, M. Elam, et al., Microwave diagnostics ahead: saving time and the lives of trauma and stroke patients, IEEE Microw. Mag. 19 (2018) 78–90.
[6] S. Semenov, J. Kellam, P. Althausen, et al., Microwave tomography for functional imaging of extremity soft tissues: Feasibility assessment, Phys. Med. Biol. 52 (2007) 5705–5719.
[7] L.E. Solberg, Ø Aardal, T. Berger, et al., Experimental investigation into radar-based central blood pressure estimation. IET Radar, Sonar Navig. 9 (2015) 145–153.
[8] S.Y. Semenov, A.E. Bulyshev, V.G. Posukh, et al., Microwave tomography for detection/imaging of myocardial infarction. I. Excised canine hearts, Ann. Biomed. Eng. 31 (2003) 262–270.
[9] D. Obeid, S. Sadek, G. Zaharia, et al., Multitunable microwave system for touchless heartbeat detection and heart rate variability extraction, Microw. Opt. Technol. Lett. 52 (2010) 192–198.
[10] C. Fu, H. Zhou, L. Tan, et al., Microwave-activated mn-doped zirconium metal–organic framework nanocubes for highly effective combination of microwave dynamic and thermal therapies against cancer, ACS Nano 12 (2018) 2201–2210.
[11] G. Abbas, M.J. Schuchert, A. Pennathur, et al., Ablative treatments for lung tumors: Radiofrequency ablation, stereotactic radiosurgery, and microwave ablation, Thorac. Surg. Clin. 17 (2007) 261–271.

[12] T. Livraghi, F. Meloni, L. Solbiati, et al., System F the CIG using A. Complications of microwave ablation for liver tumors: Results of a multicenter study, Cardiovasc. Intervent. Radiol. 35 (2012) 868–874.
[13] A.B. Copty, Y. Neve-Oz, I. Barak, et al., Evidence for a specific microwave radiation effect on the green fluorescent protein, Biophys. J. 91 (2006) 1413–1423.
[14] M. Gladovic, C. Oostenbrink, U. Bren, Could microwave irradiation cause misfolding of peptides? J. Chem. Theory Comput. 16 (2020) 2795–2802.
[15] P.G. Shields, C.C. Harris, Cancer risk and low-penetrance susceptibility genes in gene-environment interactions, J. Clin. Oncol. 18 (2000) 2309–2315.
[16] E.S. Santos, M. Blaya, L.E. Raez, Gene expression profiling and non–small-cell lung cancer: where are we now? Clin. Lung Cancer 10 (2009) 168–173.
[17] S. Son, J. Kim, J. Kim, et al., Cancer therapeutics based on diverse energy sources, Chem. Soc. Rev. 51 (2022) 8201–8215.
[18] C.J. Simon, D.E. Dupuy, W.W. Mayo-Smith, Microwave ablation: principles and applications, Radiographics 25 (2005) S69–S83.
[19] K. Komoshvili, T. Becker, J. Levitan, et al., Morphological changes in H1299 human lung cancer cells following W-Band Millimeter-wave irradiation, Appl. Sci. 10 (2020), doi:10.3390/app10093187.
[20] X. Song, C. Wang, H. Hu, et al., Microwave induces apoptosis in A549 human lung carcinoma cell line, Chin. Med. J. 124 (2011) 1193–1198.
[21] A. Zamani, S.A. Rezaeieh, A.M. Abbosh, Lung cancer detection using frequency-domain microwave imaging, Electron. Lett. 51 (2015) 740–741.
[22] S. Mumtaz, J. Lim, N.K. Kaushik, et al., in: EH Choi (Ed.), Biological Effects of Pulsed High-Power Microwaves BT - Plasma Biosciences and Medicine, Springer Nature Singapore, Singapore, 2023, pp. 281–307.
[23] J.N. Rana, S. Mumtaz, E.H. Choi, et al., ROS production in response to high-power microwave pulses induces p53 activation and DNA damage in brain cells: Radiosensitivity and biological dosimetry evaluation, Front. Cell Dev. Biol. 11 (2023), doi:10.3389/fcell.2023.1067861.
[24] M. Wang, R.S. Herbst, C. Boshoff, Toward personalized treatment approaches for non-small-cell lung cancer, Nat. Med. 27 (2021) 1345–1356.
[25] S. Mumtaz, J.S. Lim, B. Ghimire, et al., Enhancing the power of high power microwaves by using zone plate and investigations for the position of virtual cathode inside the drift tube, Phys. Plasmas 25 (2018), doi:10.1063/1.5043595.
[26] S. Mumtaz, P. Lamichhane, J. Sup Lim, et al., Enhancement in the power of microwaves by the interference with a cone-shaped reflector in an axial vircator, Results Phys. (2019) 102611.
[27] S. Mumtaz, H. Uhnm, J.S. Lim, et al., Output-power enhancement of vircator based on second virtual cathode formed by wall charge on a dielectric reflector, IEEE Trans. Electron. Devices (2022), doi:10.1109/TED.2022.3149455.
[28] S. Mumtaz, E.H. Choi, An efficient vircator with high output power and less drifting electron loss by forming multivirtual cathodes, IEEE Electron. Device Lett. 43 (2022) 1756–1759.
[29] T. Ozaki, A. Nakagawara, Role of p53 in cell death and human cancers, Cancers 3 (2011) 994–1013.
[30] D-H Lee, C. Kim, L. Zhang, et al., Role of p53, PUMA, and Bax in wogonin-induced apoptosis in human cancer cells, Biochem. Pharmacol. 75 (2008) 2020–2033.
[31] E. Hosseini, M. Ghasemzadeh, M. Atashibarg, et al., ROS scavenger, N-acetyl-L-cysteine and NOX specific inhibitor, VAS2870 reduce platelets apoptosis while enhancing their viability during storage, Transfusion 59 (2019) 1333–1343.
[32] G. Kubinyi, G. Thuróczy, J. Bakos, et al., Effect of continuous-wave and amplitude–modulated 2.45GHz microwave radiation on the liver and brain aminoacyl-transfer RNA synthetases of in utero exposed mice, Bioelectromagn. J. Bioelectromagn. Soc. Soc. Phys. Regul. Biol. Med. Eur. Bioelectromagn. Assoc. 17 (1996) 497–503.
[33] P.T. Nguyen, A.M. Abbosh, S. Crozier, 3-D focused microwave hyperthermia for breast cancer treatment with experimental validation, IEEE Trans. Antennas. Propag. 65 (2017) 3489–3500.
[34] M. Selmi, A.A. Bin Dukhyil, H. Belmabrouk, Numerical analysis of human cancer therapy using microwave ablation, Appl. Sci. 10 (2020), doi:10.3390/app10010211.
[35] J. Saranya, B.S. Sreeja, P. Senthil Kumar, Microwave assisted cisplatin-loaded CeO2/GO/c-MWCNT hybrid as drug delivery system in cervical cancer therapy, Appl. Nanosci. 13 (2023) 4219–4233.
[36] D. Manna, R. Ghosh, Effect of radiofrequency radiation in cultured mammalian cells: A review, Electromagn. Biol. Med. 35 (2016) 265–301.
[37] S. Mumtaz, P. Bhartiya, N. Kaushik, et al., Pulsed high-power microwaves do not impair the functions of skin normal and cancer cells in vitro: a short-term biological evaluation, J. Adv. Res. 22 (2020), doi:10.1016/j.jare.2019.11.007.
[38] Y. Lin, P. Gao, Y. Guo, et al., Effects of long-term exposure to L-band high-power microwave on the brain function of male mice, Biomed. Res. Int. 2021 (2021) 2237370.
[39] P. Shaw, N. Kumar, S. Mumtaz, et al., Evaluation of non-thermal effect of microwave radiation and its mode of action in bacterial cell inactivation, Sci. Rep. 11 (2021) 14003.
[40] M. Zmyślony, P. Politanski, E. Rajkowska, et al., Acute exposure to 930MHz CW electromagnetic radiation in vitro affects reactive oxygen species level in rat lymphocytes treated by iron ions, Bioelectromagnetics 25 (2004) 324–328.
[41] P. Attri, Y.H. Kim, D.H. Park, et al., Generation mechanism of hydroxyl radical species and its lifetime prediction during the plasma-initiated ultraviolet (UV) photolysis, Sci. Rep. 5 (2015) 9332.
[42] N. Takeuchi, N. Ishibashi, Generation mechanism of hydrogen peroxide in dc plasma with a liquid electrode, Plasma Sources. Sci. Technol. 27 (2018) 45010.
[43] C. Bradu, K. Kutasi, M. Magureanu, et al., Reactive nitrogen species in plasma-activated water: generation, chemistry and application in agriculture, J. Phys. D. Appl. Phys. 53 (2020) 223001.
[44] M.F. Lavin, S. Kozlov, ATM activation and DNA damage response, Cell Cycle 6 (2007) 931–942.
[45] V. Gogvadze, S. Orrenius, B. Zhivotovsky, Multiple pathways of cytochrome c release from mitochondria in apoptosis, Biochim. Biophys. Acta - Bioenerg. 1757 (2006) 639–647.
[46] M. Campioni, D. Santini, G. Tonini, et al., Role of Apaf-1, a key regulator of apoptosis, in melanoma progression and chemoresistance, Exp. Dermatol. 14 (2005) 811–818.
[47] R. Sen, A.K. Sarkar, A.K. Mandal, et al., The analysis of EM absorption for biological tissue due to RF radiation measured inside the enclosed metallic chamber, Int. Conf. Innov. Eng. Technol. 2018 (2018) 1–5.
[48] H. Matsuoka, M. Furusawa, H. Tomoda, et al., Difference in cytotoxicity of paclitaxel against neoplastic and normal cells, Anticancer Res. 14 (1994) 163–167.
[49] V. Zuco, R. Supino, S.C. Righetti, et al., Selective cytotoxicity of betulinic acid on tumor cell lines, but not on normal cells, Cancer Lett. 175 (2002) 17–25.
[50] C.-C. Wang, C.-H. Wu, K.-J. Hsieh, et al., Cytotoxic effects of cantharidin on the growth of normal and carcinoma cells, Toxicology 147 (2000) 77–87.
[51] W. Massalha, M. Markovits, E. Pichinuk, et al., Minerval (2-hydroxyoleic acid) causes cancer cell selective toxicity by uncoupling oxidative phosphorylation and compromising bioenergetic compensation capacity, Biosci. Rep. 39 (2019) BSR20181661.
[52] S. Galadari, A. Rahman, S. Pallichankandy, et al., Reactive oxygen species and cancer paradox: to promote or to suppress? Free Radic. Biol. Med. 104 (2017) 144–164.
[53] A.V. Snezhkina, A.V. Kudryavtseva, O.L. Kardymon, et al., ROS generation and antioxidant defense systems in normal and malignant cells, Oxid. Med. Cell Longev. 2019 (2019) 6175804.
[54] X. Renaudin, Chapter three - reactive oxygen species and DNA damage response in cancer, in: U Weyemi, Galluzzi LBT-IR of C and MB (Eds.), Chromatin Genomic Instab. Cancer, vol. 364, Academic Press, 2021, pp. 139–161.
[55] J.D. Hayes, A.T. Dinkova-Kostova, K.D. Tew, Oxidative stress in cancer, Cancer Cell 38 (2020) 167–197.
[56] L. Zhao, X. Zhang, X. Wang, et al., Recent advances in selective photothermal therapy of tumor, J. Nanobiotechnol. 19 (2021) 335.
[57] R. Baghban, M. Afarid, J. Soleymani, et al., Were magnetic materials useful in cancer therapy? Biomed. Pharmacother. 144 (2021) 112321.
[58] D. Sharma, K.X. Leong, G.J. Czarnota, Application of ultrasound combined with microbubbles for cancer therapy, Int. J. Mol. Sci. 23 (2022), doi:10.3390/ijms23084393.
[59] A.R. Ruiz-Fernández, L. Campos, S.E. Gutierrez-Maldonado, et al., Nanosecond Pulsed Electric Field (nsPEF): Opening the biotechnological Pandora's Box, Int. J. Mol. Sci. 23 (2022), doi:10.3390/ijms23116158.

Miss Juie Nahushkumar Rana holds a bachelor's and master's degree in biotechnology, awarded in 2016 and 2018, respectively, from Veer Narmad South Gujrat University, Surat, India. Currently, she is pursuing her Ph. D. at Kwangwoon University, Seoul, South Korea. Her research focused on the potential biological effects of high-power microwaves. Furthermore, her research also focused on the oral and other types of cancers by using nonthermal plasma and plasma-activated liquids.

Sohail Mumtaz earned his master's degree in applied physics from the Federal Urdu University of Arts, Science, and Technology (FUUAST), Islamabad, Pakistan. He completed his Ph.D. in physics at Kwangwoon University, Seoul, South Korea, in 2019 and currently serves as a research assistant professor at the same institution. His research primarily focuses on high-power microwave (HPM) generation, where he introduced an innovative approach to create multi-virtual cathodes in vircators using leaked electron wall charge. Furthermore, his work delves into exploring potential applications of HPM in the field of biology.

Eun Ha Choi is a renowned figure in the fields of plasma medicine and pulsed power technology for HPM generation within the realm of plasma physics. Currently he serves as the director of the Plasma Bioscience Research Center/Applied Plasma Medicine Center at Kwangwoon University in Seoul, Korea. He has also worked as professor and senior researcher positions at Texas Tech University (2001–2003) and Hampton University/NASA (1989–1990) and Naval Surface Warfare Center (NSWC) at MD, USA (1987–1989) in the field of plasma physics. Especially, his works on plasma medicine are focused on revolutionary breakthrough via plasma interactions with biological tissues/cells.